Peer-reviewed version available at *Appl. Sci.* **2019**, *9*, 4093; doi:10.3390/app9194093

Article

An overview of imaging lidar sensors for autonomous vehicles

Santiago Royo[1,2]* and Maria Ballesta [1]

[1] Centre for Sensor, Instrumentation and systems Development, Universitat Politècnica de Catalunya (CD6-UPC); Rambla Sant Nebridi 10 E08222 Terrassa ; santiago.royo@upc.edu
[2] Beamagine S.L.; C/Bellesguard 16 E08755 Castellbisbal, Spain;
* Correspondence: santiago.royo@upc.edu; Tel.: +34 648773478

Abstract: Imaging lidars are one of the hottest topics in the optronics industry. The need to sense the surroundings of every autonomous vehicle has pushed forward a career to decide the final solution to be implemented. The diversity of state-of-the art approaches to the solution brings, however, a large uncertainty towards such decision. This results often in contradictory claims from different manufacturers and developers. Within this paper we intend to provide an introductory overview of the technology linked to imaging lidars for autonomous vehicles. We start with the main single-point measurement principles, and then present the different imaging strategies implemented in the different solutions. An overview of the main components most frequently used in practice is also presented. Finally, a brief section on pending issues for lidar development has been included, in order to discuss some of the problems which still need to be solved before an efficient final implementation.Beyond this introduction, the reader is provided with a detailed bibliography containing both relevant books and state of the art papers.

Keywords: lidar, ladar, time of flight, 3D imaging, point cloud, MEMS, scanners, photodetectors, lasers, autonomous vehicles, self-driving car

1. Introduction

In the late years, lidar has progressed from a useful measurement technique suitable for studies of atmospheric aerosols and aerial mapping towards a kind of new Holy Grial in Optomechanical Engineering, with world class engineering teams launching start-ups, and different companies previously established in the field being acquired by large industrial corporations, mainly from the automotive and venture capital sectors. The fuel of all this activity has been the lack of an adequate solution in all aspects regarding a lidar sensor for automotive, either because of performance, lack of components, industrialization or cost issues. This has resulted in one of the strongest market-pull cases of the late years in the optics and photonics industries [1] which has even appeared in business journals such as Forbes [2], where sizes of the market in the billion unit level are claimed for the future Level 5, fully automated self driving car.

Lidar is, however, a well known measurement technique since the past century, with established publications and a dense bibliography corpus. Lidar is based in a simple working principle, based in counting the time between events in magnitudes carried out by light, such as e.g. backscattered energy from a pulsed beam, to then use the speed of light in air to compute distances or to perform mapping. Quite logically, this is referred to as the time-of flight (TOF) principle. Remote sensing has been one of the paramount applications of the technology, either from ground-based stations (e.g. for aerosol monitoring) or as aerial or spaceborne instrumentation, typically for Earth observation applications in different wavebands. A number of review papers [3], introductory text [4] or comprehensive books [5,6] have been made available on the topic across the years. Lidar has become already so relevant that a full industry related to remote sensing and mapping has been developed. The relevance of the lidar industry is shown by the existence of standars, including a dedicated data format for lidar mapping

Peer-reviewed version available at Appl. Sci. 2019, 9, 4093; doi:10.3390/app9194093

(.LAS, from laser) which has become a official standard for 3D point cloud data exchange beyond the sensor and the software managing the generated point clouds. Despite its interest and the proximity of the topic, it is not the goal of this paper to deal with remote sensing or mapping lidars, even if they provide images. They are already well-established, blooming research fields on its own with long track records, optimized experimental methods and dedicated data processing algorithms, published in specialized journals [7] and conferences [8].

However, a very relevant number of applications on the ground benefit from the capability of a sensor to capture the complete 3D information around a vehicle. Thus, still using time-counting of different events in light, first research-based, then commercial 3D cameras started to become available, and rapidly found applications in audiovisual segmentation[9], RGB+depth fusion[10], 3D screens[11], people and object detection[12] and, of course, in human-machine interfaces [13], some of them reaching the general consumer market, being the best-known example the Microsoft Kinect [14]. These commercial units were almost in all cases amplitude-modulated cameras where the phase of the emitted light was compared with the received one in order to compare their phase difference and estimate distance. A niche was covered, as solutions were optimal for indoor applications without strong solar background, and although the spatial resolution of the images was limited, and depth resolution was kept in the cm level, it was still useful for applications involving large-scale objects (like humans).

The rush towards the autonomous car and robotic vehicles pushed the requirements of the sensors into new directions. Imaging lidar sensors for automotive required a combination of long range, high spatial resolution, real time, and tolerance to solar background in daytime which pushed the technology to its limits. Different specifications with maybe different working principles appeared for the different possible use cases, including short and long range, or narrow and wide fields of view. Rotating lidar imagers were the first to achieve the required performances, using a rotating wheel configuration at high speed and multiple stacked detectors [15]. However, large-scale automotive applications required additional performance, like the capability to industrialize the sensor to achieve reliability and ease of manufacturing in order to get a final low cost unit, or to have small, nicely packaged sensor fitting in small areas of the car. It was soon obvious that different lidar sensors were required to cover all the needs of the future self-driving car, e.g. to cover short and long range 3D imaging with different needs regarding fields of view. Further, the uses of such a sensor in other markets such as robotics, defence applications, or autonomous vehicles in other markets has raised a quest for the final solid state lidar, where different competing approaches and systems have been proposed, a new proposal appears frequently, and a patent family even more frequently.

This paper intends to explain the basic aspects of imaging lidar sensors applied to autonomous vehicles, in special regarding to automotive which is the largest and fastest developing market. Due to the strong activity in the field, our goal has been more to focus on the basic details of the techniques and components currently being used, rather than to propose a technical comparison of the different solutions involved. We will however comment the main advantages and disadvantages of each approach, and try to provide further bibliography on each aspect for interested readers. Furthermore, an effort has been done in order to skip mentioning the technology used by each manufacturer, as this hardly could be complete, would be based on assumptions in some cases, and could be subject to fast changes. To those interested, there are excellent reports which identify the technology used for each manufacturer at the moment of its ellaboration [**? ?**].

The remaining of the paper has been organized as follows. Section 2 has been devoted to introduce the basics of the measurement principles of lidar, covering in a first section the three most used techniques for imaging lidar sensors, which involve pulsed beams, amplitude modulated and frequency modulated approaches. A second subsection within Section 2 will cover the strategies used to move from the point-like lidar measurement just described to an image-like measurement covering a field of view (FOV). In Section 3, we'll cover the main families of light sources and photodetectors currently used in imaging lidar units. Section 4 will be devoted to briefly review a few of the most

Peer-reviewed version available at Appl. Sci. 2019, 9, 4093; doi:10.3390/app9194093

relevant pending issues currently under discussion in the community. A final Section will outline the main conclusions of this paper.

2. Basics of lidar imaging

The measurement principle used for imaging using lidar is time-of-flight (ToF), where depth is measured by counting time delays in events in light emitted from a source. Lidar is thus an active, non-contact range-finding technique, where an optical signal is projected onto an object we call the target and the reflected or backscattered signal is detected and processed to determine the distance and thus allow the creation of a 3D point cloud of a part of the environment of the unit. Thus, the range R or distance ot the target is measured based on the round-trip delay of lightwaves which travel to the target. This may be achieved by modulating the intensity, phase, and/or frequency of the transmitted signal and measuring the time required for that modulation pattern to appear back at the receiver. In the most straightforward case, a short light pulse is emitted towards the target, and the arrival time of the pulse's echo at the detector sets the distance. This kind of pulsed lidar can provide resolutions around the centimetre level in single pulses over a wide window of ranges, as the nanosecond pulses used often have high instantaneous peak power that can reach long distances, while maintaining average power below the eye-safety limit. A second approach is based on amplitude modulation of a continuous wave (AMCW), so the phase of the emitted and backscattered detected waves is compared enabling to measure distance. A precision comparable to that of the pulsed technique can be achieved but only at moderate ranges, due to the short ambiguity distance imposed by the 2π ambiguity in frequency modulation []. The reflected signal arriving at the receiver coming from distant objects is also not as strong as in the pulsed case, as the emission is continuous, which makes the amplitude to remain below the eye-safe limit at all times. Further, digitization of the backrreflected intensity level becomes difficult at long distances. Finally, a third approach is defined by frequency-modulated continuous-wave (FMCW) techniques, enabled by direct modulation and demodulation of the signals in the frequency domain, allowing detection by coherent superposition of the emitted and detected wave. Among its main benefits it outstands its capability to achieve resolutions well below those of the other approaches, which may be down to 150μm with 1μm precision at long distances. However, its main benefit in autonomous vehicles is to obtain velocimetry measurements simultaneously to range data using the Doppler effect [16]. The three techniques mentioned are briefly discussed in the coming subsection.

2.1. Measurement principles

2.1.1. Pulsed approach

Pulsed ToF techniques are based on the simplest modulation principle of the illumination beam: distance is determined by multiplying the speed of light in a medium by the time the light takes to travel the distance to the target. Since the speed of light is constant given we stay within the same optical medium, the distance to the object is directly proportional to the travelled time. The measured time is obviously representative of twice the distance to the object, as light travels to the target forth and back, and, therefore, must be halved to give the actual range value to the target [13,17,18]:

$$R = \frac{c}{2} t_{OF} \tag{1}$$

where R is the range to the target, c is the speed of light ($c = 3.10^8$ m/s) in free space and t_{oF} is the time it takes for the pulse of energy to travel from its emitter to the observed object and then back to the receiver. Figure 1 shows a simplified diagram of a typical implementation. Further technical details of how t_{OF} is actually measured can be found in references like [17,19].

Peer-reviewed version available at Appl. Sci. 2019, 9, 4093; doi:10.3390/app9194093

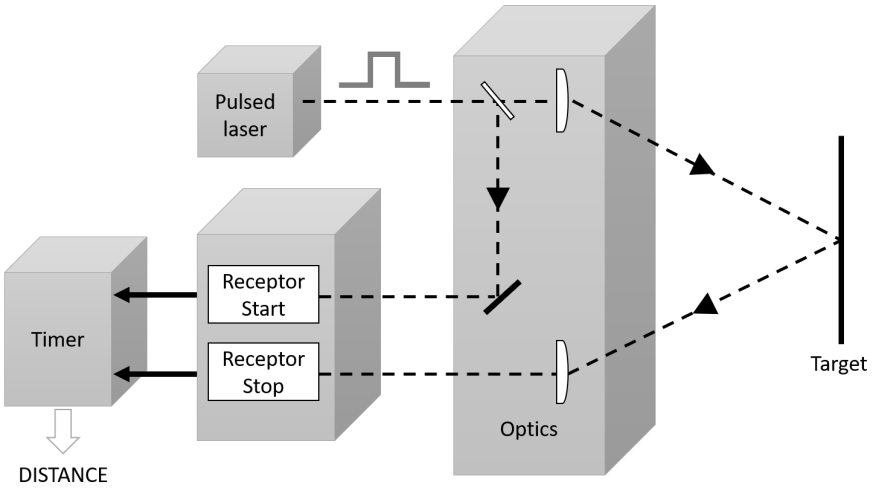

Figure 1. Pulsed TOF measurement principle

The attainable resolution in range (ΔR_{min}) is thus directly proportional to the resolution in time counting available (Δt_{min}). As a consequence, the resolution in depth measurement is dependent on the resolution in the time counting electronics. A typical resolution value of the time interval measurement can be assumed to be in the 0.1 ns range, resulting in a resolution in depth of 1.5 cm. Such values may be considered as the current reference, limited by jitter and noise in the time-counting electronics. Significant improvements in resolution may be obtained using statistics [20], but this requires several pulses per data point, degrading sensor performance in aspects like frame rate or spatial resolution.

Theoretically speaking, the maximum attainable range (R_{max}) is only limited by the maximum time interval (t_{max}) which can be measured by the time counter. However, in practice, this time interval is large enough so the maximum range becomes limited by other factors. In particular, the laser energy losses during travel (in special in diffusing targets) combined with the high bandwidth of the detection circuit (which brings on larger noise and jitter) creates a competition between the weak returning signal and the electronic noise, making the signal-to-noise ratio (SNR) the actual range limiting factor in pulsed lidars [21,22]. Another aspect to be considered concerning maximum range is the ambiguity distance (the maximum range which may be measured unambiguously), which in the pulsed approach is limited by the presence of more than one simultaneous pulse in flight, and thus is related to the pulse repetition rate of the laser. As an example, this ambiguity value ranges to 150meters at repetition rates of the laser close to the MHz range using Eq.1.

The pulsed principle directly measures the round trip time between a light pulse emission and the return of the pulse echo resulting from its backscattering off an object. Thus pulses need to be as short as possible (usually a few nanoseconds) with fast rise- and fall-times and large optical power. Because the pulse irradiance power is much higher than the background (ambient) irradiance power, this type of method performs well outdoors (although it also suitable for indoor applications, where the absence of solar background will reduce the requirements on emitted power), under adverse ambiental conditions, and can work for long-distance measurements (from a few meters up to several kilometers). However, once a light pulse is emitted by a laser and reflected onto an object, only a fraction of the optical energy may be received back at the detector. Assuming the target is an optical diffuser (which is the most usual situation), this energy is further divided among multiple scattering directions. Thus, pulsed methods need very sensitive detectors working at high frequencies to detect the faint pulses received. As long as, generally speaking, pulsed methods deal with direct energy measurements, they are an incoherent detection case [22–24].

The advantages of the pulsed approach include direct measurement of time-of-flight, its long ambiguity distance, and the limited influence of background illumination due to the use of high energy laser pulses. It is, however limited by the signal-to-noise ratio (SNR) of the measurement, where intense light pulses are required while eye-safety limits need be kept, and very sensitive detectors

Peer-reviewed version available at Appl. Sci. 2019, 9, 4093; doi:10.3390/app9194093

need be used, which may be expensive depending on the detection range. Large amplification factors in detection together with high frequency rates add on significant complexity to the electronics. The pulsed approach is, despite this limitations, the one most frequently selected in the different alternatives presented by manufacturers of imaging lidars for autonomous vehicles, due to its simplicity and its capability to perform properly outdoors.

2.1.2. Continuous Wave Amplitude Modulated (AMCW) approach

In the case of substituting the laser pulses by the intensity modulation of a continuous light wave (known as CW modulation, phase-measurement, or amplitude-modulated continuous-wave, thus AMCW) the phase-shift induced in a intensity modulated periodic signal in its round-trip to the target is used to obtain the range value. The optical power is modulated with a constant frequency f_M, typically in the tenths of MHz range, so the emitted beam is a sinusoidal or square wave of frequency f_M. After reflection from the target, a detector collects the received light signal. Measurement of the distance R is deduced from the phase shift $\Delta\Phi$ occurring between the reflected and the emitted signal [17,25,26]:

$$\Delta\Phi = k_M d = \frac{2\pi f_M}{c} 2R \Rightarrow R = \frac{c}{2}\frac{\Delta\Phi}{2\pi f_M} \tag{2}$$

where R and c are again the range to the target and the speed of light in free space; k_M is the wavenumber associated to the modulation frequency, d is the total distance travelled and f_M the modulation frequency of the amplitude of the signal. Figure 2 shows the schematics of a conventional AMCW sensor.

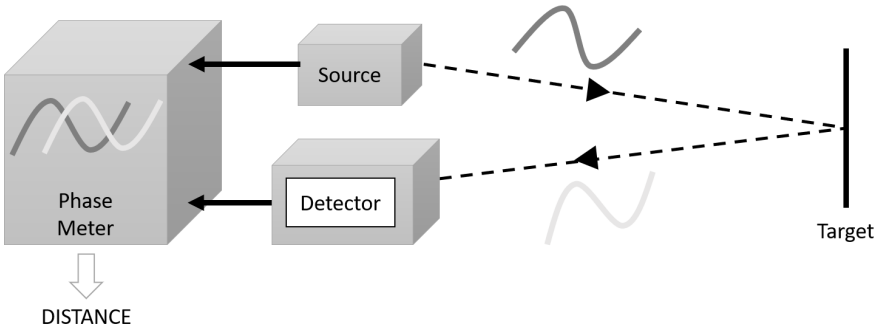

Figure 2. TOF phase-measurement principle used in AMCW lidar

There are a number of techniques which may be used to demodulate the received signal and to extract the phase information from it. For the sake of brevity, they will only be cited so the reader is referred to the linked references. For example, phase measurement may be obtained via signal processing techniques using mixers and low-pass filters [27], or, more generally, by cross-correlation of the sampled signal backscattered at the target with the original modulated signal shifted by a number (typically four) of fixed phase offsets [13,18,28,29]. Another common approach is to sample the received modulated signal and mix it with the reference signal, to then sample the resultant signal at four different phases [30]. The different types of phase meters are usually implemented as electronic circuitry of variable complexity.

In the AMCW approach resolution is determined by the frequency f_M of the actual ranging signal (which may be adjusted) and the resolution of the phase meter fixed by the electronics. By increasing f_M, the resolution is also increased if the resolution in the phase meter is fixed. However, larger f_M frequencies bring on shorter unambiguous range measurements, meaning the phase value of the return signal at different range values starts to repeat itself after a 2π phase displacement. Thus, a significant trade-off appears between the maximum unambiguity distance range and the resolution of the measurement. Typical modulation frequencies are generally in the few tenths of

Peer-reviewed version available at Appl. Sci. 2019, 9, 4093; doi:10.3390/app9194093

MHz range. Approaches using advanced modulated-intensity systems have been proposed, which deploy multi-frequency techniques to extend the ambiguity distance without reducing the modulation frequency [22].

Further, even though phase measurement may be coherent in some domains, the sensitivity of the technique remains limited because of the reduced sensitivity of direct detection in the optical domain. From the point of view of the SNR, which is also related to the depth accuracy, a relatively long integration time is required over several time periods to obtain an acceptable signal rate. In turn, this introduces motion blur in the presence of moving objects. Due to the need of these long integration times, fast shutter speeds or frame rates are difficult to obtain. [23,26].

AMCW cameras have, however, been commercialized since the 90s [31], and are referred to as TOF cameras. They are usually implemented as parallel arrays of emitters and detectors, as discussed in Section 2.2.2, being limited by the range-ambiguity trade-off, and the limited physical integration capability of the phase-meter electronics, which is done pixel by pixel or for a group of pixels in the camera, limiting the spatial resolution of the camera to a few thousands of pixels. Furthermore, AMCW modulation is usually implemented on LEDs rather than lasers, which limits the available power and thus the SNR of the signal and the attainable range, already limited by the ambiguity distance. Further, the amplitude of the signal needs be measured reliably on its arrival, and in some techniques digitized at a reasonable number of intensity levels. As a consequence, ToF cameras have little use outdoors, although they show excellent performance indoors, specially for large objects, and have been applied to a number of industries including audiovisual, interfacing and videogaming [26]. They have also been used inside vehicles in different applications, like passenger or driver detection and vehicle interfacing [32].

2.1.3. Continuous Wave Frequency Modulated (FMCW) approach

In the case of FMCW approach, the emitted instantaneous optical frequency is periodically shifted, usually by varying the power applied to the source [33]. The reflected signal is mixed with the emitted source, creating a beat frequency that is a measure of the probed distance [34]. The source is normally a diode laser to enable coherent detection. The signal is then sent to the target, and the reflected signal that arrives to the receiver, after a travelled time t_{OF} , is mixed with a reference signal built from the emitter output. For a static target (thus, with negligible Doppler effect), the delay between the collected light and the reference causes a constant frequency difference f_r, or beat frequency, between them. Letting the instantaneous frequency vary under a linear law, f_r is directly proportional to t_{OF} and hence proportional to the target range too, [25,35,36], following:

$$f_r = slope \cdot \Delta\tau = \frac{B}{T} t_{oF} = \frac{B}{T} \frac{2R}{c} \Rightarrow R = f_r \frac{cT}{2B} \tag{3}$$

where B is the bandwidth of the frequency sweep, T denotes the ramp of the ramp in the modulation frequency, and $\Delta\tau$ equals the total travelled time t_{oF}. Figure 3 represents all these parameters. In practice, the frequency difference between the outgoing and incoming components is translated into a periodic phase difference between them, which causes an alternating constructive and destructive interference pattern at the frequency f_r, i.e. a beat signal at frequency f_r. By using FFT to transform the beat signal in time domain to frequency domain, the peak of beat frequency is easily translated into distance.

Peer-reviewed version available at Appl. Sci. 2019, 9, 4093; doi:10.3390/app9194093

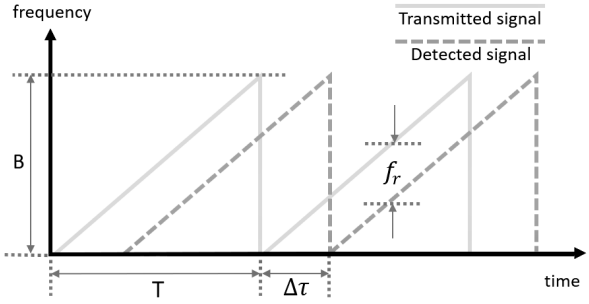

Figure 3. Frequency modulation and detection in the FMCW method: main parameters

Usually, a triangular frequency modulation is used (Figure 4) rather than a ramp. The modulation frequency in this case is denoted as f_m. Hence, the rate of frequency change can be expressed as $2f_mB$ [37], and the resulting beat frequency is given by:

$$f_r = \frac{4Rf_mB}{c} \tag{4}$$

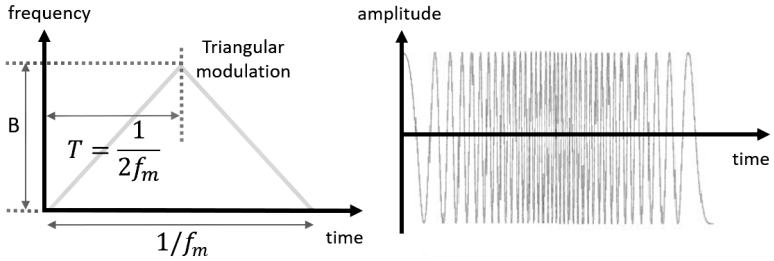

Figure 4. Triangular frequency modulation with time and linked amplitude signal change in the time domain

This type of detection has the very relevant advantage to add on the capability of measuring not only range but also, on the same signal, the velocity of the target. If the target moves, the beat frequency obtained will not only be related to R, but also to the velocity v_r of the target relative to the sensor. The velocity contribution is taken into account by the Doppler frequency f_d, which will affect the sweep of the beat frequency up or down. Thus, beat frequency components are superimposed to f_r, following [38]:

$$f^+ = f_r + f_d \text{ and } f^- = f_r - f_d \tag{5}$$

Peer-reviewed version available at Appl. Sci. 2019, 9, 4093; doi:10.3390/app9194093

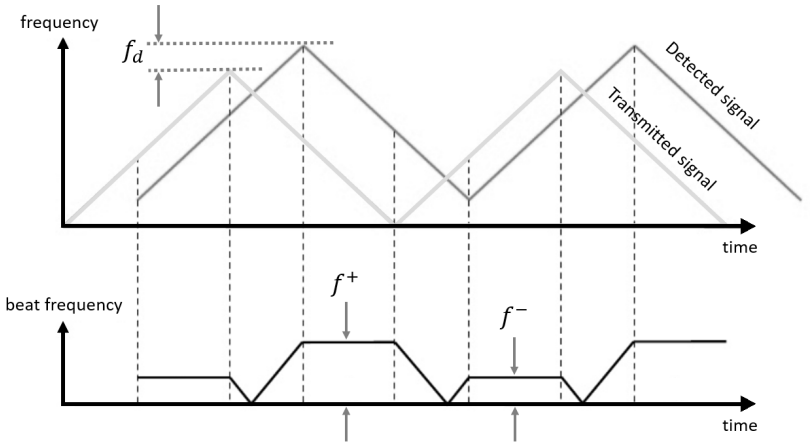

Figure 5. Triangular modulation frequency signal and beat frequency for a moving target

In this case, range can be obtained from:

$$R = \frac{cT}{4B}\left(f^+ + f^-\right) \tag{6}$$

while relative velocity and its direction can also be calculated using the Doppler effect:

$$v_r = \frac{\lambda}{2} f_d = \frac{\lambda}{4}\left(f^+ - f^-\right) \tag{7}$$

showing the ability of FMCW to simultaneously measure range and relative velocity using the properties of the Fourier spectra. [37,39].

FMCW takes advantage of the large frequency bandwidth available in the optical domain and exploits it to improve the performance of the range sensor. The resolution of the technique is now related to the total bandwidth of the signal. Since the ramp period can be chosen arbitrarily, the FMCW method can determine t_{OF} values in the picosecond range, equivalent to millimeter or even submillimeter distances, by performing frequency measurements in the kilohertz regime, which is perfectly feasible. Resolutions of 150μm have been reported, which is an improvement of two orders of magnitude relative to Unfortunately, in general, a perfect linear or triangular optical frequency sweep cannot be realized by a linear modulation of the control current and, in addition, the frequency versus control current characteristic is in general nonlinear, in special close to the moment of slope change. As a consequence, deviations from the linear ramp usually occur which, in turn, bring on relevant variations in f_r. Moreover, the range resolution depends on the measurement accuracy of f_r and also on the accuracy with which the modulation slope is controlled or known [16,25,35].

The FMCW method is fundamentally different from the two previous approaches because of the use of the coherent (homodyne) detection scheme in the Fourier domain, rather than the incoherent intensity detection schemes described until now for time counting or phase emasurement approaches [16]. FMCW has shown to be useful in outdoor environments and to have improved resolution and long range values relative to the pulsed and AMCW approaches. However, its coherent detection scheme poses potential problems related to practical issues like coherence length (interference in principle requires the beam to be within coherence length in the full round-trip to the target), availability of durable tunable lasers with good temperature stability, external environmental conditions, accuracy of the modulation electronics, or linearity of the intensity-voltage curve of the laser, which require advanced signal processing. Although it is not a majoritary approach in imaging lidars for autonomous vehicles, some teams are currently implementing lidar solutions based on FMCW in commercial systems due to its differential advantages, and clearly winning presence when compared to the rest of approaches we described.

Peer-reviewed version available at Appl. Sci. 2019, 9, 4093; doi:10.3390/app9194093

2.1.4. Summary

The three main measurement principles use share its goal of measuring TOF, but have very different capabilities and applications. The pulsed approach is limited by SNR, the measurement principle is incoherent, as it is based in the detection of intensity, and can show resolutions at the cm level, being operative under strong solar background. Its main advantage is the simplicity of the setup, stable, robust and with available general purpose components. The main disadvantage involves the limit in range due to low SNR and the emision limit fixed by eye-safety levels. AMCW methods have been commercialized several years ago and are exceptionally well developed and efficient in indoor environments, with stable electronics designs working in parallel based on CMOS technology. They present equivalent resolution to those of pulsed lidars, and the complexity of determining the reliability of the phase measurements using low SNR signals. Finally, the FMCW approach presents relevant advantages which appear to place them as the natural choice for autonomous vehicles, as its coherent detection scheme enables improvements in resolution of range measurements between 1 and 2 orders of magnitude when cmpared to the other methods, and specially beacuse the use of FFT signal processing enables to measure speed of the target simultaneously. Despite this advantages, it is a coherent system which needs to be significantly stable in its working conditions to be reliable, and aspects like temperature drift or linearity of electronics become significant, which is significant in an application which demands robustness and needs units performing stably for several years.

2.2. Imaging strategies

Once the three main measurement strategies used in imaging lidar sensors have been presented, it is worth noting all of them have been presented as pointwise measurements. However, lidar images of interest are always 3D point clouds, which achieve accurate representations of fields of view as large as 360º around the object of interest. A number of strategies have been proposed in order to build lidar images out of the repetition of pointwise measurements, but they essentially may be grouped in three different families or its combinations: scanning components of different types, detector arrays, and mixed approaches. Scanning systems are used to sweep a broad number of angular positions of the field of view of interest using some beam steering component, while detector arrays exploit the capabilities of electronic integration of detectors to create an array of receiving elements, each of one capturing illumination from separate angular sections of the scene to deliver a $t_o f$ value per individual detector. Some of the strategies have also been successfully combined with each other depending on the measurement approach or requirements, which are discusssed in a Section devoted to mixed approaches.

2.2.1. Scanners

Currently, in the automotive lidar market most of the proposed commercial systems rely on scanners of different types. [40–43]. In the most general approach, the scanner element is used to re-position the laser spot on the target by modifying the angular direction of the outgoing beam, in order to generate a point cloud of the scene. This poses questions related to the scanning method, its precision, its speed, its field of view, and its effect on the beam footprint on the target, which directly affects the spatial resolution of the images [44].

A large number of scanning strategies have been proposed for lidar and laser scanning and are currently effective in commercial products (such as e.g galvanometric mirrors [45] or Risley prisms [46]). When it comes to its use in autonomous vehicles, four main categories may be found: mechanical scanners, as described, which use rotating mirrors, galvanometric positioning and prisms to perform the scanning; MEMS scanners, which use electromechanically actuated micromirrors to scan the field of view sometimes supported by expanding optics, and optical phased arrays, which perform pointing of the beam based on a multibeam interference principle. Direct comparisons of scanning strategies for particular detector configurations have been proposed [41]. Although we will focus on these four large

Peer-reviewed version available at Appl. Sci. 2019, 9, 4093; doi:10.3390/app9194093

families, it is worth noting that other approaches have been proposed based on alternative working principles such as liquid crystal waveguides [47], electrowetting [48], groups of microlens arrays [49] and even holographic diffraction gratings [50].

a) Mechanical scanners. Imaging lidar sensors based on mechanical scanners use high-grade optics and some kind of rotating or galvanometric assembly, usually with mirrors or prisms attached to mechanical actuators, to cover a wide field of view. In the case of lidar units with sources and detectors jointly rotating around a single axis This may be done by sequentially pointing the beam across the target in 2D, as depicted in Figure 6, or by rotating the optical configuration around a mechanical axis, in which case a number of detectors may be placed in parallel along the spinning axis. In this latter case 360deg FOVs of the sensor may be achieved,covering the whole surroundings of the vehicle. The mirrors or prisms used may be thus rotating or oscillating, or may be polygon mirrors. This is the most popular scanning solution for many commercial lidar sensors, as it provides straight and parallel scan lines with a uniform scanning speed over a vast FOV [51,52], or angularly equispaced concentric data lines, In rotating mirrors, the second dimension is usually obtained by adding more sources and/or detectors to measure different angular directions simultaneously. Further, the optical arrangement for rotating lidar units may be simple and extremely efficient in order to collect faint diffuse light and thus achieve very long ranges as there is some margin in the size of the collection optics, specially when compared to other approaches.

Lidars with mechanical scanners work almost always with pulsed sources and are usually significantly large and bulky. In the case of rotating mirrors, they can achieve large spatial resolution in the direction of turn (usually horizontal) although they become limited in the orthogonal direction (usually vertical) where the density of the point cloud is limited by the number of available sources measuring in parallel. Further, they need rather high power consumption and, due to the large inertia of the rotating module, the frame rate is limited (frame rate goes from below 1 Hz to about 100 Hz). They are, however, very efficient in long range applications (polygon mirrors combined with coaxial optical systems easily reach distances well beyond 1 km). Despite the current prevalence of these type of scanners, the setup presents numerous disadvantages in a finlal consumer unit, in particular the question of reliability and maintenance of the mechanisms, the mass and inertia of the scanning unit which limits the scanning speed, the lack of flexibility of the scanning patterns, and the issue of being misalignment-prone under shock and vibration, beyond being power-hungry, hardly scalable, bulky and expensive. Although several improvements are being introduced in this systems [42] there is a quite general agreement that mechanically scanning lasers need to move towards a solid-state version. However, they are currently providing one of the closest performance available for the final long-range lidar unit, and they are commercially available from different vendors using modified principles. This makes them the sensor of choice for autonomous vehicle research and development, such as algorithm training [53], autonomous cars [54], or robotaxis [55]. Their success also has brought a number of improvements in geometry, size and spatial resolution to make them more competitive as final imaging lidar in automotive.

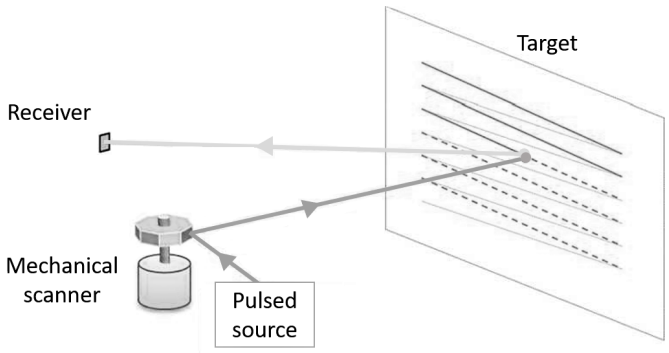

Figure 6. Diagram of a typical imaging lidar based on mechanical scanning

Peer-reviewed version available at Appl. Sci. 2019, 9, 4093; doi:10.3390/app9194093

b) Microelectromechanical scanners.

Microelectromechanical system (MEMS) based lidar scanners enable programmable control of laser beam position using tiny mirrors a few mm in diameter whose tilt angle varies when applying a stimulus, so the angular direction of the incident beam is modified and the light beam is directed to a specific point in the scene. This may be done bidimensionally (in 2D) so a complete area of the target is scanned. Various actuation technologies are developed including electrostatic, magnetic, thermal and piezoelectric. Depending on the applications and the required performance (regarding scanning angle, scanning speed, power dissipation or packaging compatibility), one or another technology is chosen. The most common stimulus in lidar applications based on MEMS scanners is voltage: the mirrors are steered by drive voltages generated from a digital representation of the scan pattern stored in a memory. Then, digital numbers are mapped to analog voltages with a digital-to-analog converter. However, electro-magnetic and piezoelectric actuation has also been successfully reported for lidar applications [51,56–58].

Thus, MEMS scanners substitute mechanical-scanning hardware with an electromechanical equivalent reduced in size. Because they have no rotating mechanical components, a reduced FOV is obtained compared to the previously described rotary scanners, which enabled up to 360^{o} . However, using multiple channels and fusing their data allows to create FOVs and point cloud densities able to rival or improve mechanical lidar scanners [59,60]. Further, MEMS scanners have typically resonance frequencies well above those of the vehicle, enhancing maintenance and robustness aspects.

MEMS scanning mirrors are categorized into two classes according to their operating mechanical mode: resonant and non-resonant. On one hand, non-resonant MEMS mirrors (also called quasi-static MEMS mirrors) provide a large degree of freedom in the trajectory design. Although a rather complex controller is required to keep the scan quality, desirable scanning trajectories with constant scan speed at large scan ranges can be generated by an appropriate controller design. Unfortunately, one key spec such as the scanning angle is quite limited in this family compared to resonant MEMS mirrors. Typically, additional optomechanics are required in order to enlarge the scan angle, adding optical aberrations like distortion to the scanning angle. On the other hand, resonant MEMS mirrors provide a large scan angle at a high frequency and a relatively simple control design. However, the scan trajectory is sinusoidal, i.e. the scan speed is not uniform. However, their design needs to strike a balance where the combination of scan angle, resonance frequency, and mirror size is combined for the desired resolution, while still keeping the mirror optically flat to avoid additional image distortions which may affect the accuracy of the scan pattern [51,61,62].

A 2D laser spot projector can be implemented either with a single biaxial mirror or using two separate, orthogonal uniaxial mirrors. Uniaxial scanners are simpler to design and fabricate, and are also far more robust to vibration and shock; however, biaxial scanners provide important optical and packaging advantages, essentially related to simplicity of the optical arrangement and accuracy required in the relative alignment of the two uniaxial mirrors. One crucial difficulty with dual-axis scanners is the crosstalk between the two axes. With the increasing requirements of point cloud resolution it becomes harder to keep the crosstalk to acceptable levels, which would be a reason to choose the bulkier and more complex two-mirror structure. The most common system architecture is raster scanning, where a low frequency, linear vertical scan (quasi-static) is paired with an orthogonal high frequency, resonant horizontal scan. For the raster scanner the fast scanner will typically run at frequencies of some KHz (typically exceeding 10 KHz), and should provide a large scan angle.[62,63].

A detailed overview on MEMS Laser Scanners is provided in [61], where the topics covered previously may be found expanded. Extended discussions on accuracy issues in MEMS mirrors may be found in [62].

Due to its promising advantages (in particular light-weight, compact and low power consumption) MEMS-based scanners for lidar have received increasing interest for their use in automotive applications. MEMS-based sensors have in parallel showed the feasibility of the technology in various application such as space applications and robotics. Currently, the automotive

Peer-reviewed version available at Appl. Sci. 2019, 9, 4093; doi:10.3390/app9194093

lidar utilization of MEMS is under development by a number of companies [43,51,64–67] becoming one of the preferred solutions of choice at present.

d) Optical phased arrays.

An optical phased array (OPA) is a novel type of solid-state device that enables to steer the beam using a multiplicity of micro-structured waveguides. Its operating principle is equivalent to that of microwave phased arrays, where the beam direction is controlled by tuning the phase relationship between arrays of transmitters. By aligning the emitters' phases of several coherent emitters, the emitted light interferes constructively in the far field at certain angles. While phased arrays in radio were first explored more than a century ago, optical beam steering by phase modulation has been demonstrated first in the late 1980's [68–71].

In an OPA system, an optical phase modulator controls the speed of light passing through the device. Regulating the speed of light enables control of the shape and orientation of the wave-front resulting forom the combination of the emission from the synced waveguides. For instance, the top beam is not delayed, while the middle and bottom beams are delayed by increasing amounts at will. This phenomenon effectively allows the deflection of a light beam, steering it towards different directions. OPAs can achieve very stable, rapid, and precise beam steering. Since there is no mechanical moving parts at all, they are robust and insensitive to external constraints such as acceleration, allowing extremely high scanning speed over 100 kHz over large angles. Moreover, they are highly compact and can be single chip. However the insertion loss of the laser power is a drawback, [4,72] as their current ability to handle the large power densities required for long-range lidar imaging.

OPAs have gained interest in recent years as an alternative to traditional mechanical beam steering or MEMS-based techniques, because they completely lack inertia, which limits the ability to reach a large steering range at a high speed, and because the steering elements may be integrated with an on-chip laser. As a developing technology with high potential, the interests on OPA for automotive lidar is growing in academia and industry even though OPAs are still under test for long range lidar, although they are operative in some commercially available units targetting shorter and mid ranges [73]. Recently, sophisticated OPAs have been demonstrated with performance parameters that make them seem suitable for high power lidar applications [70,74,75]. The combination of OPAs and FMCW detection has got the theoretical potential to drive a lidar system fully on chip, which becomes one of the best potential combinations for a lidar unit, given both technologies develop at the required pace and no major roadblocks are found in the development.

2.2.2. Detector arrays

Due to the lack of popularity in the automotive market of scanning lidar approaches based on moving elements, alternative imaging methods have been proposed to overcome their limitations. Those scannerless techniques typically combine specialized illumination strategies with arrays of receivers. Transmitting optical elements illuminate a whole scene and a linear array (or matrix) of detectors receive the signals of separate angular subsections in parallel, allowing to obtain range data of the target in a single shot (see Figure 8) making easy to manage real-time applications. The illumination may be pulsed (flash imagers) or continuous (AMCW or FMCW lidars). With the exception of FMCW lidars, where coherent detection enables longer ranges, flash imagers or imagers based on AMCW principle (known as TOF cameras) are limited to medium to short ranges. In flash lidars the emitted light pulse is dispersed in all directions, significantly reducing the SNR, while in ToF cameras the phase ambiguity effect limits the measured ranges to a few meters. Eye-safety considerations are significant is this flood illumination aproaches, also[51]. A brief description of the basic working principle is provided next.

Peer-reviewed version available at Appl. Sci. 2019, 9, 4093; doi:10.3390/app9194093

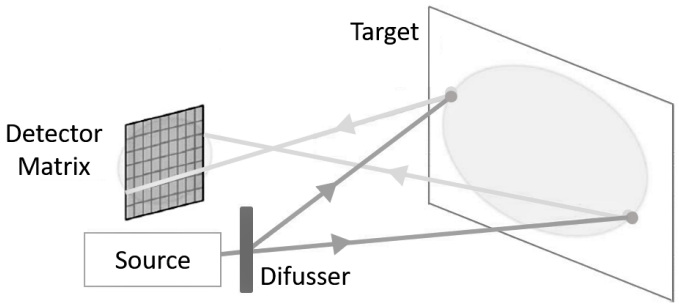

Figure 7. Detector array-based lidar diagram

a) Flash imagers.

One very successful architecture in transport systems is flash lidar, which has progressed to a point where it is very close to commercial deployment in short and medium range systems. In a flash lidar, imaging is obtained by flood-illuminating a target scene or a portion of a target scene using pulsed light. The backscattered light is collected by the receiver which is divided among multiple detectors. Detectors capture the image distance, and sometimes the reflected intensity using the conventional time-of-flight principle. Hence, both, the optical power imaged onto a 2-D array of detectors and the 3-D point cloud, are directly obtained with a single laser blast on the target. [44,76,77]. Area detectors thus need area illuminators.

In a flash-lidar system, the FOV of the array of detectors needs to closely match the illuminated region on the scene. This is usually achieved using an appropriate divergent optical system which expands the laser beam to illuminate the full FOV. The beam divergence of the laser is usually arranged to optically match the receiver FOV, allowing to illuminate all the pixels in the array at once. Each individual detector in the array is individually triggered by the arrival of a pulse return and measures both its intensity and range. The spatial resolution thus strongly depends on the resolution of the camera, that is, on the density with which the detectors have been packed, usually limited by CMOS technology. The resolution in z depends, usually, on the pulse width and the accuracy of the time counting device. Typically, the spatial resolution obtained is not very high due to the size and cost of the focal plane array used. Values around some tenths of Kpx are used [41], limited by cost and size of the detector (as they usually work at 1.55μm, and are thus InGaAs based. Resolution in depth and angular resolution are comparable to scanning lidars, even better insome arrangements.

Since the light intensity from the transmitter is dispersed with a relatively large angle to cover the full scene, and such a value is limited by eye-safety considerations, the measurement distance is dependent on sensing configurations, including aspects like emitted power, sensor FOV and detector type and sensitivity. It can vary from tenths of meters to very long distances, although at present they are used in the 20m to 150m range in automotive. Range and spatial resolution of the measurement obviously depend on the FOV considered for the system, which limits the entrance pupil of the optics and the area where the illuminator needs to spread power enough for detectivity. The divergence of the area illuminator and the backscattering at the target significantly reduce the amount of optical power avilable, so very high peak illumination power and very sensitive detectors are required if comparison to single-pixel scanners is required, to illuminate the entire scene while keeping eye safety limits and still see far enough. Detectors are usually APDs working in the Geiger mode regime enabling single photon detection, known as SPADs (Single Photon Avalanche diodes) This has caused that at present flash setups have been kept concentrated in sensing at medium or short range applications in autonomous vehicles, where they take advantage of their lack of moving elements, and they have acceptable costs in mass production due to the simplicity of the setup [51].

The main disadvantage of flash imagers, however, comes from the type of response of the detectors used, which are used in Geiger mode and thus produce a flood of electrons at each detection. Combined with the presence of retroreflectors in the real-world environment, in particular in roads

Peer-reviewed version available at Appl. Sci. 2019, 9, 4093; doi:10.3390/app9194093

and highways where they are routinely used in traffic signs and license plates. Retroreflectors are designed to reflect most of the light and backscatter very little to be visible at night when illuminated by the car headlamps. In practice retroreflectors flood the detector with photons, saturating it, and blind the entire sensor for some frames, rendering it useless. Some schemes based on interference have been proposed to skip such problems [78]. Issues related to mutual interference of adjacnt lidars, so one lidar detects the illumination of the other, are also expected to be a problem hard to solve in flash imagers. On the other hand, since flash lidars capture the entire scene in a single image, the data capture rate can be very fast so the method is more immune to vibration effects and movement artifacts which could distort the image. Hence, flash lidars have proven to be useful in specific applications such as tactical military imaging scenarios where both the sensor platform and the target move during the image capture, a situation also common in vehicles. Other advantages include elimination of scanning optics and moving elements and potential for creating a miniaturized system [79,80]. This has resulted in systems based on flash lidars effectively being commercialized for automotive at present [81].

b) AMCW cameras.

A second family of imaging lidars which use detector arrays are the TOF cameras based on the AMCW measuring principle. As described in Section 2.1.2, these devices modulate the intensity of the source and then measure the phase difference between the emitter and the detected signal at each pixel on the detector. This is done by sampling the returned signal at least four times. Detectors for these cameras are often manufactured using standard CMOS technology, so they are small and low-cost, based on well-known technology and principles, and capable of short-distance measurements (from a few centimeters to several meters) before they enter into redundancy issues due to the priodicity of the modulation. Typical AMCW lidars with a range of 10m may be modulated at around 15 MHz, thus requiring that the signal at each pixel be sampled at around 60 MHz. Most commercially available TOF cameras operate by modulating the light intensity in the near infrared (NIR), and use arrays of detectors where each pixel or group of pixels incorporates its own phase meter electronics. This in practice poses a maximum value on the spatial resolution of the scenes to the available capabilities of lithographic patterning, being most of them limited to some tenths of thousands of points per image. It is a limit comparable to that of the flash array detectors just mentioned, also due to manufacturing limitations. However, TOF cameras perform susully in the NIR region, so their detectors are based in silicon, while flash imagers are usually working at 1.55μm for eye-safety considerations. The AMCW strategy is less suitable for outdoor purposes due to the effects of background light on SNR and the number of digitization levels needed ot reliably measure the phase of the signal. However, they have been widely used indoor in numerous other fields such as robotics, computer vision, and home entertainment [82]. In automotive, they have been proposed for occupant monitoring in the car. A detailed overview of current commercial TOF cameras is provided in [13].

2.2.3. c) Mixed approaches.

Some successful proposals of lidar imagers have mixed the two imaging modalities presented above, that is, they have combined some scanning approach together with some multiple detector arrangement. The cylindrical geometry enabled by a single rotating axis combined with a vertical array of emitters and detectors has been very successful [**?**] to parallelize the conventional point scanning approach both in emission and detection, and thus increase data and frame rate while enabling for each detector a narrow field of view, which makes them very efficient energetically and thus able to reach long distances. A comparable approach has also been developed for flash lidars, with an array of detectors and multiple beams mounted on a rotating axis [83]. These cylindrical detector approaches obviously demand line-shaped illumination of the scene. They may enable 360deg vision of the FOV, in difference with MEMS or flash approaches which only retrieve the image within the predefined FOV of the unit.

Peer-reviewed version available at Appl. Sci. 2019, 9, 4093; doi:10.3390/app9194093

Another interesting and succesful mixed approach has been to use 1D MEMS mirrors for scanning a projected line onto the target, which is then recovered by either cylindrical optics on a 2D detector array, or onto an array of 1D detectors [84]. This significantly reduces size and weight of the unit while enabling large point rates, and provides very small and efficient sensors without macroscopic moving elements.

2.2.4. d) Summmary

the single-point measurement strategies used for lidar need imaging strategies to deliver the desired 3d maps of the surrounding in the vehicle. We divided them into scanners and detector arrays. While mechanical scanners are now prevalent in the industry, the presence of moving elements supposes a threat to the duration and reliability of the unit in the long term, due to sustained shock and vibration conditions. MEMS scanners appear to be the alternative, as they are lightweight, compact units with resonance frequencies well above those typical in a vehicle. They can scan large angles using adapted optical systems and use little power. They however present problems related to linearity of the motion and heat dissipation. OPAs would be the ideal solution, providing static beam steering, but they present problems in the management of large power values, which set them currently in the research level. However, there are commercial low-power systems commercially using OPAs, so they are a fesible alternative for the future.

On the detector array side, flash lidars provide a good solution without any moving elements, specially in the close and medium ranges, where they achieve comparable performance figures to scanning systems. Large spatial resolution in InGaAs is however expensive, and the use of detectors in Geiger mode poses issues related to the presence of retrorreflective signs which can temporarily blind the sensor. The AMCW approach, as described, is based in detector arays but is not reliable enough in outdoor environments. Intermediate solutions combining scanning using cylindrical geometries (rotation around an axis) with line illuminators and linear detector arrays along a spinning axis have also been proposed, both using the point-shaped beams and the flash approach.

We do not want to finish this Section without mentioning an alternative way of classifying lidar sensors which by now should be obvious to the reader. We preferred an approach based on the components utilized for building the images, as it provides an easier connection with the coming Sections. However, an alternative classification of lidars based on how they illuminate the target would have also been possible, dividing them into those who illuminate the target point by point (scanners), as 1D lines (like the cylindrical approach just described) or as a simultaneous 2D flow (flash imagers or TOF cameras). Such a classification also enables to include all the different families of imaging lidars. An equivalent classification based on the detection strategy (single detector, 1D array, 2D array) would also have been possible.

3. Sources and detectors for imaging lidars in autonomous vehicles

Lidar systems illuminate a scene and use the backscattered signals that returns to a receiver for range-sensing and imaging. The basic system thus must include a source or transmitter, a sensitive photodetector or receiver, the data processing electronics, and a strategy to obtain the information of all the target, essential for the creation of the 3D maps and/or proximity data images. We have just discussed the main imaging strategies, and the data processing electronics used are usually specialized regarding their firmware or code, but there is not really a specialized choice of technology for these components in general. Data processing and device operation are usually managed by variable combinations of Field Programmable Gate Arrays (FPGAs), Digital Signal Processors (DSPs), microcontrollers or even computers depending on the system architecture. Efforts oriented to dedicated chipsets for lidar are emerging and have reached the commercial level [**?**], although they still need of dedicated sources and detectors.

Thus, we believe the inclusion of a dedicated section to briefly review the sources and detectors used in imaging lidar is required to complete this review. Due to the strong requirements on frame rate,

Peer-reviewed version available at Appl. Sci. 2019, 9, 4093; doi:10.3390/app9194093

spatial resolution and signal to noise ratio imposed to imaging lidars, light sources and photodetectors become key state of the art components of the system, subject to strong development efforts, and which have different trade-offs and performance issues when used in lidar.

3.1. Sources

Lidars usually employ sources with wavelengths from the infrared region, typically from 0.80 to 1.55μm to take advantage of the atmospheric transmission window, and in particular of water, at those wavelengths [**?**], while enabling the use of beams not visible to the human eye. The sources are mainly used in three regions: a waveband from 0.8μm to 0.95μm, dominated by diode lasers which may be combined with silicon-based photodetectors; lasers at 1.06μm, still usable for Si detectors and usually based on fibre lasers, and lasers at 1.55μmm, available from the telecom industry, which may be either diode laser or fibre lasers, but which need InGaAs detectors. Those these are the most usual cases, other wavelengths are possible, as the lidar detection principle is general and works in most cases regardless the wavelength selected. Wavelength is in general selected taking into account considerations related to costs and eye safety. 1.55μm, for instance, enables much more power within the eye safety limit defined by Class 1 [**?**] but may become really expensive if detectors need to be above the conventional telecom size (200μm).

Sources are thus based either on lasers or on nonlinear optical systems driven by lasers; although other sources may be found (such as LEDs), usually for short-range applications. Different performance features must be taken into account in order to select the most suitable source according to the system purpose. This includes, as the most relevant for automotive, peak power, pulse repetition rate (PRR), pulse width, wavelength (including purity and thermal drift), emission (single mode, beam quality, CW/pulsed), size, weight, power consumption, shock resistance and operating temperature. In one very typical feature of imaging lidars, such performance features may involve trade-offs for a given technology; for instance, a large peak power typically goes against a large PRR or spectral purity.

Currently, the most popular sources for use in lidar technology are solid state lasers (SSL) and diode lasers (DLs), with a few exceptions. SS lasers employ insulating solids (crystals, ceramics, or glasses) with elements added (dopants) that provide the energy levels needed for lasing. A process called optical pumping is used to provide the energy for exciting the energy levels and creating the population inversion required for lasing. Generally, SSL use DLs as pumping source to create the population inversion needed for lasing. The use of SSLs for performing active-sensing for range-finding started in 1960 with the SS ruby laser, thanks to the development of techniques to generate nanosecond-duration pulses. Since then, almost every type of laser has been employed in demonstrations for this application. SSLs can be divided into a wide range of categories, for example bulk or fiber, with this latter having increasingly became prevalent in lidar for autonomous vehicles, not only because of its efficiency and capacity for generation of high average powers with high beam quality and PRR, but also because it provides an easy way to mount and align the lidar using free-space optics.

Increasing attention has been devoted to microchip lasers. They are, perhaps, the ultimate in miniaturisation of diode-pumped SSLs. Their robust and readily mass-produced structures are very attractive. Combining this characteristic with other of their features, such as their single-frequency CW performance or their excellence at generating sub-nanosecond pulses make microchip lasers well suited for many applications, being lidar among them. They need free-space alignment, in difference with fibres, but can also achieve large peak energies with excellent beam quality. A more detailed description of all these laser sources, and of some others less relevant to lidar, can be found in [44].

Semiconductor DLs, finally, are far more prevalent in the industry due to their lower cost and their countless applications beyond lidar. They are considered to be a separate laser category, although they are also made from solid-state material. In a DL, the population inversion leading to lasing takes place in a thin layer between a semiconductor PN junction, named the depletion zone, where under electrical polarization the recombination of electrons and holes produces photons, which get

Peer-reviewed version available at Appl. Sci. 2019, 9, 4093; doi:10.3390/app9194093

confined inside the depletion region. This provides lasing without the need of an optical pump, so DLs can directly convert electrical energy into laser light output, making them very efficient. Different configurations are available for improved performance, including Fabry-Perot cavities, Vertical-Cavity Surface emitting Lasers, distributed feedback lasers, etc. [**?**].

3.1.1. Fiber lasers

Fiber lasers are usually meant to be lasers that use optical fibers as the active media for lasing. The optical fiber is doped with rare earth elements (such as Er^{+3}) and one or several fiber-coupled DLs are used for pumping. In order to turn the fiber into a laser cavity, it is needed some kind of reflector (mirror) to form a linear resonator, or to build a fiber ring architecture. For commercial products, it is common to use a Bragg grating at the edge of the fiber which allows to reflect back part of the photons. Although, in broad terms, the gain media of fiber lasers is similar to that of SS bulk lasers, the wave-guiding effect of the fibre and the small effective mode area usually lead to substantially different properties. For example, they often operate with much higher laser gain and resonator losses [85–88].

Fiber lasers can have very long active regions, and so they can provide very high optical gain. Currently, there are high-power fiber lasers with outputs of hundreds of watts, sometimes even several kilowatts (up to 100 kW in continuous wave operation) from a single fiber [**?**] . This potential arises from two main reasons: on one side, from a high surface-to-volume ratio, which allows efficient cooling because of the low and distributed warming; on the other side, the guiding effect of the fibre avoids thermo-optical problems even under conditions of significant heating [**?**]. The fiber's waveguiding properties also permit the production of a diffraction-limited spot, that is, the smallest spot possible due to the laws of Physics, with very good beam quality enabling a very small divergence of the beam linked only to the numerical aperture of the fibre, which stays usually within 0.1deg values. [89,90]. This divergence is proportional to the footprint of the beam on the target, and thus is directly related to spatial resolution of the lidar image.

Furthermore, due to the fact that light is already coupled into a flexible fiber, it is easily delivered to a movable focusing element allowing convenient power delivery and high stability to movement. Moreover, fibre lasers also enable configurable external trigger modes to ease the system synchronization and control, and have compact size because the fiber can be bent and coiled to save space. Some other advantages include its reliability, the availability of different wavelengths, their large PRR (1 MHz is a typical value) and their small pulse width (< 5 ns). Fibre lasers provide a good balance between peak power, pulse duration and pulse repetition rate, very well suited to imaging lidar specifications. Nowadays, its main drawback at present is its cost, which is much larger than other alternatives even in volume [44].

3.1.2. Microchip lasers

Microchip laser are bulk SS lasers with a piece of doped crystal or glass working as gain medium. Its design allows optical pump power to be transmitted into the material, as well as to spatially overlap the generated laser power with the region of the material which receives the pumping energy. The ability to store large amounts of energy in the laser medium is one of the key advantages of bulk SS lasers, and is unique to them. A saturable absorber (active or passive) induces high losses in the cavity until the energy storage saturates (passive) or is actively liberated by means of a shutter (active Q-switch) [91,92].

The active medium of microchip lasers is a millimeter-thick, longitudinally pumped crystal (such as Nd:YAG) directly bonded to solid media that have saturable absorption at the laser wavelength. This transient condition results in the generation of a pulse containing a large fraction of the energy initially stored in the laser material, with a width that is related to the round-trip time of light in the laser cavity. Due to their short laser resonator and thus very short round-trip time combined with bulk energy storage, microchip lasers are well suited to the generation oh high power short pulses,

Peer-reviewed version available at Appl. Sci. 2019, 9, 4093; doi:10.3390/app9194093

well beyond the needs of conventional lidar specs. Simple contruction methods are enough to obtain short pulses in the nanosecond-scale (typical < 5 ns). Q-switched microchip lasers may also allow the generation of unusually short pulses with duration below 1 ns, although this poses problems in the amplification electronics. Particularly with passive Q-switching, it is possible to achieve high PRR in the MHz region combined with short pulses of few ns, very well suited to present lidar needs. For lower repetition rates (around 1 KHz), pulse energies of some microjoules and pulse duration of a few nanoseconds allow for peak powers of multiple kilowatts (> 1 kW). Beam quality can be very good, even diffraction-limited [93–96].

Microchip lasers provide an acceptable balance between peak power and pulse duration in a compact and cost-effective design in scale production. They have found their own distinctive role, which make them very suitable for a large number of applications. Many of these applications benefit from a compact and robust structure; and the small electric power consumption. In other cases, their excellence at generating sub-nanosecond pulses and/or the possible high pulse repetition rates are of interest. For example, in laser range-sensing, it is possible to achieve a very high spatial resolution (down to 10 cm or less) due to the short pulse duration [97,98]. Cost stays midway between DL and fiber lasers, although closer to the fiber side.

3.1.3. Diode lasers

There are two major types of DL: interband lasers, which use transitions from one electronic band to another, and quantum cascade lasers (QCL), which operate on intraband transitions relying on an artificial gain medium made possible by quantum-well structures built using band structure engineering. DL are by far the most widespread in use, but recently, QCL have emerged as an important source of mid and long-wave infrared emission [4,44,99].

Interband DL are electrically pumped semiconductor lasers in which the gain is generated by an electrical current flowing through a PN junction or (more frequently) with a Pdoped-Insulator-N doped (PIN) structure to improve performance. A PIN junction properly polarized makes the I-region the active media, expanding the depletion zone where carriers can recombine releasing energy as photons, and acting as waveguide for the generated photons. The goal is to recombine all electrons and holes to create light confined by edge mirrors of the I region, one of them partially reflective so the radiation can escape form the cavity. This process can be spontaneous, but can also be stimulated by incident photons, efectively leading to optical amplification, and to laser oscillation given external optical feedback is provided [100–103].

Interband lasers can be presented in a number of geometries that correspond to systems operating in very different regimes of optical output power, wavelength, bandwidth, and other properties. Some examples include edge-emitting laser (EEL), vertical-cavity surface-emitting DL (VCSEL), distributed feedback (DFB) lasers, high-power stacked diode bars or external cavity DL. Many excellent reviews exist discussing the characteristics and applications of each of these types of laser [44,104–108].

Regarding lidar applications, DL have the advantage of being cheap and compact. Although they provide less peak power than fibre or microchip lasers it is still enough for lidar applications (maximum peak power may be up to the 10kW range) [109]. However, they become limited by a reduced pulse repetition rate ($\sim$300kHz) and pulse width ($\sim$100 ns). Furthermore, high-power lasers are usually in the EEL configuration, yielding a degraded beam quality with a fast and a slow axis diverging differently, which negatively affects the laser footprint and the spatial resolution. However, they are currently used in almost every lidar either on their own, or used as optical pumps in SS lasers [110], and they are extremely good regarding their cost against peak power figure of merit, a specially sensitive one in automotive applications.

3.2. Photodetectors

Along with light sources, photodetectors are the other main component of a lidar system which has dedicated features. The detector element is the critical photon sensing device in an active receiver

Peer-reviewed version available at Appl. Sci. 2019, 9, 4093; doi:10.3390/app9194093

which enables the TOF measurement. It needs to have large sensitivity for direct detection of intensity, and it also has to be able to detect short pulses, thus requiring high bandwidth. A wide variety of detectors are available for lidar imaging, ranging from single-element detectors to arrays of 2D detectors, which may build an image with a single pulse [111].

The material of the detector defines its sensitivity to the wavelength of interest, so currently Si-based detectors are used for the waveband between 0.3μm and 1.1μm, While InGaAs detectors are used above 1.1μm, although they have good sensitivities from 0.7μm and beyond [**?**]. InP detectors and InGaAs/InP heterostructures have also been proposed as detectors in the mid-infrared [112], although their use in commercial lidar systems is rare due to their large cost if outside telecommunications standards and, eventually, the need for cooling them to reduce their noise figure.

Light detection in imaging lidars usually account for four different detector types: PIN diodes, avalanche photodiodes (APD), single-photon avalanche photodiode (SPAD) and the photomultiplier tube (PMT). Each one may be built from the material which addresses the wavelength of interest. .

The most used single-detectors are PIN photodiodes, which may be very fast detecting events in light if they have enough sensitivity for the application, but do not provide any gain inside of their media. For applications that need moderate to high sensitivity and can tolerate bandwidths below the GHz regime typical of PIN diodes, avalanche photodiodes (APDs) are the most useful receivers as their structure provides a certain level of multiplication of the current generated by the incident light. APDs are able to increase internally the current generated by the photons incident in the sensitive area, providing a level of gain, usually around two orders of magnitude, but they are linear devices with gain which provide a current output proportional to the optical power received. Single-photon avalanche diodes (SPAD) are essentially APD biased beyond the breakdown voltage and with their structure arranged to repetitively withstand large avalanche events. Whereas in an APD a single photon can produce in the order of tens to few hundredths of electrons, in a SPAD a single photon produces a large electron avalanche which results in detectable photocurrents. An interesting arrangement of SPADs has been proposed in the shape of Multi-Pixel Photon Counters (MPPC), which are pixelated devices formed by an array of SPADs where all pixel outputs are added together in a single analog output, effectively enabling photon counting through the measurement of the fired intensity. [44,113–115]. Finally, PMTs are based on the external photoelectric effect and the emission of electrons within a vacuum tube which brings them to collision with cascaded dinodes, resulting in a true avalanche of electorns. Although they are not solid state, they still provide the largest gains available for single photon detection and are sensitive to UV, which may make them useful in very specific applications. Their use in autonomous vehicles is rare, but they have been the historical detector of reference in atmospheric or remote sensing lidar [116]. Several complete overviews of photodetection, photodetector types, and their key performance parameters may be found elsewhere and go beyond the scope of this paper [44,117–120]. Here we'll focus only in main photodetectors used in imaging lidars. Due to the relevance of the concepts of gain and noise in imaging lidars, where SNR ratios in detection are usually small, only a brief discussion on the concepts of gain and noise will be introduced here before getting into the detailed descrption of the different detector families of interest.

3.2.1. Gain and noise

As described above, gain is a critical ability of a photodetector in low SNR conditions as it enables to increase the available signal. Gain increases the power or amplitude of a signal from the input (in lidar, the initial number of photoelectrons generated by the absorbed incoming photons) to the output (the final number of photoelectrons sent to digitization) by adding energy to the signal. It is usually defined as the mean ratio of the input signal to the output power, so a gain greater than 1 indicates amplification. On the other side, noise includes all the unwanted irregular fluctuations produced by the detector and associated electronics which accompany the signal, and perturb the detectivity of the actual useful signal by obscuring it. Photodetection noise may be due to different parameters well described in [121].

Peer-reviewed version available at Appl. Sci. 2019, 9, 4093; doi:10.3390/app9194093

Gain is a relevant feature of any photodetector in low SNR applications. Conventionally, a photon striking the detector surface has some probability of producing a photoelectron, which in turn produces a current within the detector which usually is converted to voltage and digitized after some amplification circuitry. The gain of the photodetector dictates how many electrons are produced by each photon which are successfully converted into a useful signal. The effect of this detectors in the signal to noise ratio of the system is to add a gain factor G to both the signal and certain noise terms, which may also be amplified by the gain.

Noise is, in fact, a deviation of the signal; so it is represented by a standard deviation (σ_{noise}). A combination of independent noise sources is then the accumulation of its standard deviations,which means that a dominant noise term is likely to appear :

$$\sigma_{noise} = \sqrt{\sigma_{shot}^2 + \sigma_{th}^2 + \sigma_{back}^2 + \sigma_{read}^2 + ...} \tag{8}$$

Thermal noise σ_{th} and shot noise σ_{shot} are considered fixed system noise sources. The first is due to the thermal motion of the electrons inside the semiconductor, which adds electrons not related to the incident optical power to the measured current; and the second to the statistical fluctuations in the optical signal itself and the statistical interaction process. Shot noise is more relevant in very low light applications, where the statistics of photon arrival become observable. Other noise sources are considered as external, such as background noise σ_{back}, readout noise σ_{read}, or speckle noise $\sigma_{speckle}$. they respectively appear as a consequence of the existence of background illumination in the same wavelength of the laser pulses, fluctuations in the generation of photoelectrons or its amplification, or the presence of speckle fluctuations in the received laser signal. While fixed system noise will not be affected by the gain of the detector, background, readout and speckle noise will also be amplified by the gain, which may become counter productive. When either thermal or shot noise are the dominant noise sources we are in the thermal or shot noise regimes of a detector and the existence of gain improves significantly the SNR of the detector.

The SNR for a detector with gain may then be written as:

$$SNR_{APD} \approx \frac{G \cdot N_{signal}}{\sqrt{\sigma_{shot}^2 + \sigma_{th}^2 + G^2 \cdot \sigma_{back}^2 + G^2 \cdot \sigma_{read}^2 + ...}} \tag{9}$$

where N_{signal} is the number of photoelectrons generated by real incoming photons. Equation 9 shows the advantage to work in thermal or shot regime regarding gain. In those cases SNR is effectively improved by increasing the signal power.

3.2.2. Photodetectors in imaging lidar

a) PIN photodiodes

A PIN photodiode is a diode with a wide, undoped intrinsic semiconductor region between a p- and a n-doped regions. When used as a photodetector, the PIN diode is reverse-biased. Under this condition the diode is not a conductor, but when a photon of sufficient energy enters the depletion region it creates an electron-hole pair. The field of the reverse bias then sweeps the carriers out of the region creating a current proportional to the number of incoming photons. This gives rise to a photocurrent sent to an external amplification circuit. The depletion region stays completely within the intrinsic region, and is much larger than in a PN diode and almost constant-sized, regardless of the reverse bias applied to the diode.

As receivers, most of photons are absorbed in the I-region, and carriers generated therein can efficiently contribute to the photocurrent. They can be manufactured with multiple different materials including Si, InGaAs, CdTe,...yielding wide options regarding their spectral response, although the most usual single-element detectors used are Si and InGaAs PIN photodiodes. PIN photodiodes do not have any gain (G=1), but may present very large bandwidths (up to 100GHz, depending on its size

Peer-reviewed version available at Appl. Sci. 2019, 9, 4093; doi:10.3390/app9194093

and capacitance), dimensions of millimeters, low cost, low bias and large QE. However, due to their features they are not suitable for low light applications. In imaging lidar sensors, they are typically used as detectors in pulsed lidars to raise the start signal for the time-to-digital converter at the exit of the laser pulse.

b) Avalanche photodiodes

An avalanche photodiode (APD) is a diode-based photodetector with an internal gain mechanism that is operated with a relatively high reverse bias voltage (typically tens or even hundredths of volts), sometimes just below breakdown of the device, hich happens when a too large reverse bias is applied on the device. As with a conventional photodiode detector, absorption of incident photons generates a limited number of electron-hole pairs. While under high bias voltage, a strong internal electric field is created which accelerates the carriers generated and creates additional secondary electrons, in this case by impact ionization. The resulting electron avalanche process, which takes place over a distance of only a few micrometers, can produce gain factors up to few hundredths but is still directly proportional to the incoming optical power. The amplification factor of the APD dictates the number of photoelectrons that are created with the successful detection of each photon, and, thus, the effective responsivity of the receiver. Gain may vary from device to device and strongly depends on the reverse voltage: the higher the reverse voltage, the higher the gain. However, if the reverse voltage is increased further, a voltage drop occurs due to the current flowing through the device load resistance. This means that the value of the maximum gain has a dependence on the photocurrent. Although there is a large linear region of operation where the output photocurrent presents gain but is still proportional to the power of the incoming light, when the APD is operated near its maximum gain (and thus close to the breakdown voltage) the APD response is not linear anymore, and the APD is said to operate in Geiger mode. The level of gain required to obtain the optimal SNR value may thus be dependent on the amount of incident light. Several excellent reviews of APDs in detail are available [122].

APDs are very sensitive detectors. However, the avalanche process itself creates fluctuations in the generated current and thus noise, which can offset the advantage of gain in the SNR. The noise associated with the statistical fluctuations in the gain process is called excess noise. Its amount depends on several factors: the magnitude of the reverse voltage, the properties of the material (in particular, the ionization coefficient ratio), and the device design. Generally speaking, when fixed system noise is the limiting noise factor the performance of APDs is much better than devices with ordinary PIN photodiodes. However, increasing gain also increases the excess noise factor, so there exists an optimal operating gain for each operating conditions, usually well below the actual maximum gain, where the maximum SNR performance can be obtained.

Linear-mode APDs (in contrast to Geiger-mode APDs or SPADs, described in next Section) present output signals amplified by a gain and proportional to the incoming light. Compared to PIN photodiodes, they have comparable bandwidth, but can measure lower light levels, and thus may be used in a variety of applications requiring high sensitivity, such as long-distance communications, optical distance measurements, and obviously for lidar. However, they are not sensitive enough for single-photon detection. They are a mature and widely available technology, so APDs are also available in array-form, in multiple sizes, either 1D or 2D arrays, with photosensitive areas up to 10×10 mm, specially in Si. Large InGaAs arrays, on the contrary, are hard to find and prohibitively priced.

c) Single photon avalanche photodiodes

APDs working in Geiger-mode are known as single-photon avalanche diode (SPADs). SPADs are operated slightly above the breakdown threshold voltage, being the electric field so high that a single electron-hole pair injected into the depletion layer can trigger a strong, self-sustained avalanche. The current rises swiftly to a macroscopic steady level and it keeps flowing until the avalanche can be *quenched*, meaning it is stopped and the SPAD is operative again. Under this circumstances, the

Peer-reviewed version available at Appl. Sci. 2019, 9, 4093; doi:10.3390/app9194093

photocurrent is not linearly amplified, but rather a standard final value is reached whether it has been triggered by only one or many carrier pairs. The design of the device architecture needs be prepared for repeated avalanches without compromising the response of the detector. The structure of SPADs is different from those of linear mode APDs in order to withstand repeated avalanches and have efficient and fast quenching mechanisms.

For an effective Geiger-mode operation the avalanche process must be stopped and the photodetector must be brought back into its original quiescent state. This is the role of the quenching circuit. Once the photocurrent is triggered, the quenching circuit reduces the voltage at the photodiode below the breakdown voltage for a short time, so the avalanche is stopped. After some recovery time, the detector restores its sensitivity and is ready for the reception of further photons. Such a dead-time constitutes a substantial limitation of this devices, as it limits the count rate and leaves the device unuseful for times in the 100ns band, limiting the bandwidth of SPADs. This is being tackled through improved quenching circuits. Currently two types of quenching are in use: passive, in which avalanche is interrupted by lowering the bias voltage below breakdown using a high-value resistor as described; and active, based on active current feedback loops. Active quenching was specifically devoted to overcome the slow recovery times characteristic of passive quenching. The rise of the avalanche is sensed through a low impedance and a reaction back on the device is triggered by controlling the bias voltage using active components (pulse generators or fast active switches) that force the quenching and reset transitions in shorter times[123]. Active quenching is a very active research line currently due to its relevance in low light detection in several imaging applications [124].

The macroscopic current generated due to the avalanche is discernible using electronic threshold detection. Since threshold detection is digital, it is essentially noiseless, although there exist different mechanisms that can also fire the avalanche process generating noise. The main sources of false counts in SPADs are thermally-generated carriers and afterpulsing [125]. The first case is due to the generation-recombination processes within the semiconductor due to thermal fluctuations, which may induce the avalanche and produce a false alarm. In the second case, during the avalanche, some carriers are captured by deep energy levels in the junction depletion layer and subsequently released with a statistically fluctuating delay. Released delayed carriers can retrigger the avalanche generating these after-pulses, an effect that increases with the delay of avalanche quenching and with the current intensity.

SPADs are, however, extremely efficient in low light detection, and can be used when an extremely high sensitivity at the single photon detection level is required. Devices with optimized amplifier electronics are also available in CMOS integrated form, even as large detector arrays, in applications from quantum optics to low-light biomedical imaging. The intensity of the signal may be obtained by repeated illumination cycles counting the number of output pulses received within a measurement time slot. Statistical measurements of the time-dependent waveform of the signal may be obtained by measuring the time distribution of the received pulses, using the time-correlated single photon counting (TCSPC) technique [20]. SPADs are used in a number of lidar applications and products, taking advantage of its extreme sensitivity, and may be found individually, or in 1D or 2D arrays . Their main drawback is their sensitivity to large backreflections which may saturate the detector and leave it inoperative for short periods, an event easily found in real life where large retroreflective signs are present almost everywhere on the road as traffic signs. Methods to mitigate this effect are already being proposed [126].

d) Multipixel photon counters

SPADs are very efficient in the detection of single photons, but they provide a digital output delivering just the presence of one or more photons, or its absence. The signal obtained when detecting one or several photons is equivalent,which is a drawback in several applications. Multipixel photon counters (MPPCs), also known as Silicon Photomultipliers (SiPMs) are essentially SPAD arrays with cells of variable size, but which recombine the output signal of each individual SPAD into a joint analog

Peer-reviewed version available at Appl. Sci. 2019, 9, 4093; doi:10.3390/app9194093

signal[127,128]. In such a fashion, the analog signal is proportional to the amount of SPADs triggered, potentially enabling photon counting beyond the digital photon detection capability presented by SPADs.

Each microcell in a MPPC consists of a SPAD sensor with its own quenching circuit. When a microcell triggers in response to an absorbed photon, the Geiger avalanche causes a photocurrent to flow through the microcell. The avalanche is confined to the single pixel where it was initiated while all other microcells remain fully charged and ready to detect photons. When a photon is detected, the receiving unit in the array outputs a single pulse with a fixed amplitude that does not vary with the number of photons entering the unit at the same time. The output amplitude is equal for each of the pixels. Although the device works in digital mode pixel by pixel, MPPCs become analog devices as all the microcells are read in parallel and each of the pulses generated by multiple units are superimposed onto each other to obtain the final photocurrent. A a drawback, linearity gets worse as more photons are incident on the device, because the probability for more than one photon hitting the same microcell increases. Further, as an array the potential for crosstalk and afterpulsing between cells may be significant depending on the application [129]. Optical crosstalk occurs when a primary avalanche in a microcell triggers secondary discharges in one or more adjacent microcells, i.e., the unit that actually detects photons affects other pixels making them produce pulses that make the output signal higher than that implied by the amount of the incident light. Its probability depends on fixed factors (like the size of the microcell and the layered architecture) and variable ones like the difference between the bias voltage being appplied and the breakdown voltage.

A typical MPPC has microcell densities of between 100 and several 1000 per mm^2, depending upon the size of the unit. Its characteristics greatly vary depending on the operating voltage and ambient temperature. In general, raising the reverse voltage increases the electric field inside the device and so, improves the gain, photon detection efficiency and time resolution. On the other hand, as seen before, it also increases undesired components which lower the SNR, such as false triggers due to thermal noise and afterpulsing. Thus, the operating voltage must be carefully set in order to obtain the desired characteristics.

Despite these practicalities, MPPCs have many attractive features including very high gains (about 10^6), analog photon-counting capabilities, a wide number of available commercial sizes (they are even modular so they can be attached next to each other), and in particular lower operation voltages and power consumptions than the ones required for conventional PMT. Due to its characteristics, it is a potential device for many low light applications, in particular for lidar or in any singlephoton application where solid state detectors are an advantage related to PMTs.

e) Photomultiplier tubes

As a final detector in the series, photomultiplier tubes (PMTs) have played and still play a relevant role in several applications, including atmospheric lidar for remote sensing. Although their features (volume, price) are not useful for autonomous vehicles, we'll cover them briefly for completeness of low light detection. They have been compared to MPPC detectors in lidar showing comparable performance [116].

PMTs are based in the external photoelectric effect. A photon incides onto a photosensitive area within a vacuum tube which extracts a photoelectron from the material. Such photoelectron is accelerated to impact onto a cascaded series of electrodes named dynodes, where more electrons are generated by ionization at each impact creating a cascaded secondary emission. Each photoelectron generated is multiplied in cascade enabling again single-photon detection. It is possible to obtain gains up to 10^8 at MHz rate [130].

PMTs have dominated the single-photon detection scene for many years, in special in scientific and medical applications, as they are the only photodetectors with decent response and gain in the UV region, present unrivalled gain and their rise time is in the ns scale, so their bandwidth is very large ($>$ 1 GHz). However, PMTs are bulky devices which are not solid state and are affected by

Peer-reviewed version available at Appl. Sci. 2019, 9, 4093; doi:10.3390/app9194093

magnetic fields, which strongly limits their applicability in autonomous vehicles. Other disadvantages include the requirement for a high-voltage supply, the high cost and, in some cases, their low quantum efficiency.

4. Pending issues

While the deployment of imaging lidars for autonomous vehicles seems unstoppable, and major automotive manufacturers are starting to select providers for data collection units and introducing them in commercial vehicles, the final technology implementation is still uncertain in several relevant details. The selection of the most appropriate technology and scanning strategy among the different competing alternatives in terms of cost and functionality still needs in-depth work, and becomes one of the most visible examples of the current uncertainty in the industry. However, beyond the final technology of choice there are still several relevant issues which need be worked out for full implementation of imaging lidars in vehicles. Here we present a list of pending issues to be solved for final implementation of imaging lidars in vehicles,in particular considering automotive. A complete list of all potential pending issues is impossible to compile, but we propose what seem to us some very relevant problems for lidar deployment, most of them general to all types of measurement principles and implementations.

4.1. Spatial resolution

Dense point clouds with large spatial resolution both in the horizontal and vertical directions are one of the cornerstones of object detection. While detectivity at long range has been achieved even for objects with low reflectivities, the reliable identification of objects at significant distances needs enhancement, as shown by the trend in larger and larger spatial resolution [131]. A rule-of-thumb number says objects above 10cm can hit the bumper of some cars, and braking or evasion at highway speeds needs at least detection hazards at 150m. This brings on a spatial resolution of This means a spatial resolution of 0.67mrad for detecting a point on the object. If five to ten points are considered for reliable identification of an object, then spatial resolution in all directions need be reduced to just 67μrad, a number which is insanely small. Although cumulative detection procedures, statistics and machine learning may help to improve detection [132], it is still clear that larger spatial resolutions, in special along the vertical axis, will be required if autonomous vehicles need to drive at fast speeds on highways. Approaches with spatial resolution close to 1mrad in horizontal and vertical directions preserving real-time operation start to be available [67].

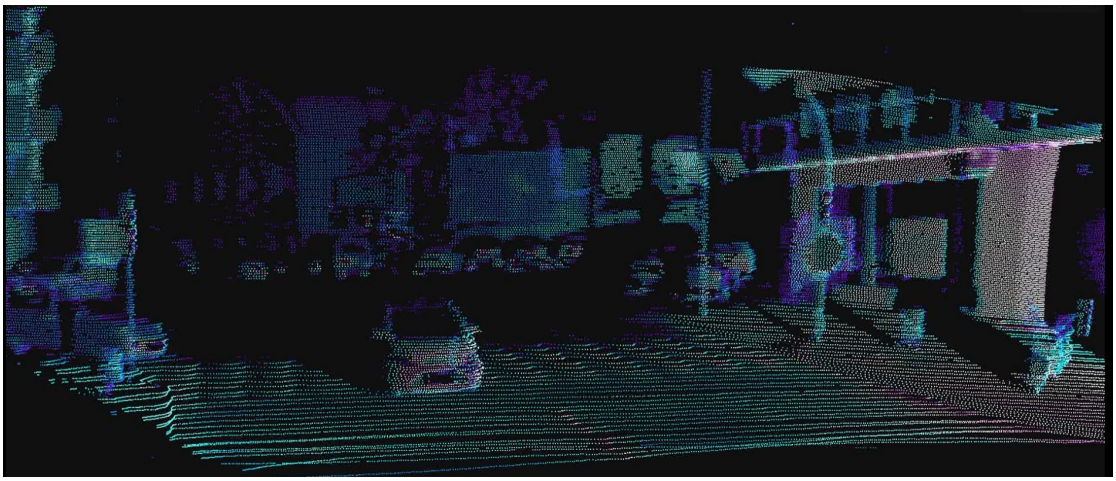

Figure 8. Lidar imaging with 1mrad spatial resolution in vertical and horizontal directions[67]

Peer-reviewed version available at Appl. Sci. 2019, 9, 4093; doi:10.3390/app9194093

4.2. Sensor fusion and data management

Despite lidar may be in the headlines, a complex sensor suite involving a number of sensor is expected to be required. Such sensors need to have complementary measurement principles and failure modes to get a safe and reliable solution for fully autonomous cars [133]. In general, short and long range radar and lidar, combined with ultrasound and vision cameras are generally accepted as parts of the potential solution. Such amount of information, without including the high density point clouds just mentioned above, need be fused and processed in real time to detect hazards and react timely to them [134]. Such amount of information has been estimated to be somewhere between 11TB and 140Tb per day, with bandwidths in the range of $19TB/h$ to $40Tb/h$ [135], which becomes a relevant storage, processing and management problem by itself. Regarding sensor fusion procedures, they may be dependent on the operative conditions of the moment, but even with this assumption processes are not obvious, involving different approaches for different lidar principles: fusing information from a camera and a mechanical scanning lidar covering 360deg is harder than in the limited FOV of a voice coil or MEMS scanner. Such procedures are not obvious as soon as parallax errors due to the different position and geometry of the sensors are prone to appear, while posing demanding requirements on the computing power of the vehicle in any case, even for embedded solutions.

4.3. Sensor distribution

If the components of the sensor suite are still under definition and in an early stage within the production cycle for manufacturing, its potential distribution along the vehicle is not a simple decision to take. The number of sensors reasonably mounted on the self-driving car is estimated to be somewhere between 20 and 40 [135]. Further, data collection and machine learning procedures may become affected by relevant changes in the point of view, in the worst cases forcing the tedious data collection process to be started again. It is generally accepted that the current approach taken for robotaxis in controlled environments or data collection vehicles, with lidars and sensors fixed on the roof of the vehicle is not acceptable for commercial units. Where to place the lidar, if not on the roof, has relevant implications related to covered FOV and number of units required, with the associated cost consequences. The decision has relevant implications also on the vehicle itself, where currently not much free space is available for sensors. Further, position of sensors is key for aspects such as reliability, dirt management, servicing or survival of the unit after minor crashes. Despite the most usual approach is to embed the lidar in the central front pannel of the vehicle, there are alternatives such as e.g headlamps as potential lodging of lidar sensors [136].

4.4. Bad weather conditions

Autonomous driving tests are, up to now, handled mostly in sunny environments, such as California or Texas. However, the quality of the detection under fog, rain and snow, in special if they are extreme, becomes severely degraded in special regarding range [137] due to the absorption and scattering events induced by water droplets. This introduces a large number of false detection alarms from backscattered intensity, reducing the reliability of the sensor [83,138]. Further, snowflakes, fog and rain droplets have different shapes, distributions and sizes and affect different aspects of the detection, complicating a precise modelling [139]. Managing imaging lidar detection in extreme weather conditions is a pending subject of the technology which need be tackled in the near future for commercial deployment of automated vehicles.

4.5. Mutual interference

To close this section, let's consider a world full of self-driving cars each with its lidar emitting pulses or waves. Imagine them in a traffic jam, or in an area with large vehicle density. The uniqueness of the signal emitted by each lidar needs be ensured, so the source of one vehicle does not trigger the detection in other vehicles in their surroundings. Although some approaches may have advantages

Peer-reviewed version available at Appl. Sci. 2019, 9, 4093; doi:10.3390/app9194093

the implementation of discrimination patterns among each individual vehicle may be demanding [140]. For instance, FMCW dtection appears to be better than direct pulse detection as the modulation frequency and amplitude, combined with the coherent detection implemented, may help to add personalized signatures to each lidar. However, the implementation of this concept at mass scale needs be carefully considered, and possibly supported by improved data processing to filter out false detections.

5. Conclusions

Imaging lidars are a novel type of sensor enabling 3D perception of our environment, and not just the conventional 2D projection obtained from a camera. Within this paper we have tried to describe in detail the different configurations of imaging lidar sensors available for atutonomous vehicles. Despite discussion becomes biased towards cars, similar considerations the the ones presented here may be stated for maritime or aerial vehicles. We reviewed and compared the three main working principles subjacent to all lidar measurements, to then overview the main strategies involved in imaging, grouped into scanners (mechanical, MEMS and OPAs) and detector arrays (flash and TOF approaches). Afterwards, we tried to overview the principal sources and photodetectors used in lidar units at present, showing its advantages and disadvanatages. We finished with some of the most relevant pemnding issues which imaging lidar in vehicles needs to overcome to become the reality everyone is expecting.

The desired goal of the paper was to order somehow the disparity of information delivered by lidar manufacturers, scientific papers, proceedings and market studies in the field, sometimes quite biased due to commercial needs and venture capital pressure. They are very exciting times for imaging lidars, a field where mechanics, optronics, software and robotics are merging to develop, potentially, the social revolution which autonomous vehicles may bring. Possibly, the less uncertain thing is we can wait for several surprises along the way.

The authors wish acknowledge the support from Dr.Jan-Erik Kallhammer and Dr.Jordi Riu in the revsion and ellaboration of this manuscrips, and the financial support received from MINECO projects FIS2017-89850R, from EU in project H2020-826600-VIZTA, and from AGAUR through Grant 2019FI-B-00868.

References

1. Woodside Capital Partners and Yole Développement. Automotive LiDAR Market Report. OIDA Publications & Reports, 2018.
2. Schoonover, D. The Driverless Car Is Closer Than You Think–And I Cant́ Wait. Forbes, 2019.
3. Comerón, A.; Muñoz-Porcar, C.; Rocadenbosch, F.; Rodríguez-Gómez, A.; Sicard, M. Current research in LIDAR technology used for the remote sensing of atmospheric aerosols. *Sensors* **2017**, *17*, 1450.
4. McManamon, P.F. Field Guide to Lidar. SPIE, 2015.
5. Weitkamp, C. LiDAR: introduction. In *Laser remote sensing*; CRC Press, 2005; pp. 19–54.
6. Dong, P.; Chen, Q. *LiDAR remote sensing and applications*; CRC Press, 2018.
7. Remote Sensing – Open Access Journal. https://www.mdpi.com/journal/remotesensing.
8. Remote Sensing – Events. https://www.mdpi.com/journal/remotesensing/events.
9. Douillard, B.; Underwood, J.; Kuntz, N.; Vlaskine, V.; Quadros, A.; Morton, P.; Frenkel, A. On the segmentation of 3D LIDAR point clouds. 2011 IEEE International Conference on Robotics and Automation. IEEE, 2011, pp. 2798–2805.
10. Premebida, C.; Carreira, J.; Batista, J.; Nunes, U. Pedestrian detection combining rgb and dense lidar data. 2014 IEEE/RSJ International Conference on Intelligent Robots and Systems. IEEE, 2014, pp. 4112–4117.
11. Neumann, U.; You, S.; Hu, J.; Jiang, B.; Lee, J. Augmented virtual environments (ave): Dynamic fusion of imagery and 3d models. IEEE Virtual Reality, 2003. Proceedings. IEEE, 2003, pp. 61–67.
12. Himmelsbach, M.; Mueller, A.; Lüttel, T.; Wünsche, H.J. LIDAR-based 3D object perception. Proceedings of 1st international workshop on cognition for technical systems, 2008, Vol. 1.

Peer-reviewed version available at Appl. Sci. 2019, 9, 4093; doi:10.3390/app9194093

13. Kolb, A.; Barth, E.; Koch, R.; Larsen, R. Time-of-flight cameras in computer graphics. Computer Graphics Forum. Wiley Online Library, 2010, Vol. 29, pp. 141–159.
14. Han, J.; Shao, L.; Xu, D.; Shotton, J. Enhanced computer vision with microsoft kinect sensor: A review. *IEEE transactions on cybernetics* **2013**, *43*, 1318–1334.
15. Moosmann, F.; Stiller, C. Velodyne slam. 2011 ieee intelligent vehicles symposium (iv). IEEE, 2011, pp. 393–398.
16. Behroozpour, B.; Sandborn, P.A.; Wu, M.C.; Boser, B.E. Lidar system architectures and circuits. *IEEE Communications Magazine* **2017**, *55*, 135–142.
17. Illade-Quinteiro, J.; Brea, V.; López, P.; Cabello, D.; Doménech-Asensi, G. Distance measurement error in time-of-flight sensors due to shot noise. *Sensors* **2015**, *15*, 4624–4642.
18. Sarbolandi, H.; Plack, M.; Kolb, A. Pulse Based Time-of-Flight Range Sensing. *Sensors* **2018**, *18*, 1679.
19. Theiß, S. Analysis of a pulse-based ToF camera for automotive application. *Master's thesis* **2015**.
20. O'Connor, D. *Time-correlated single photon counting*; Academic Press, 2012. Google-Books-ID: ELQ0Mz6Rq1EC.
21. Koskinen, M.; Kostamovaara, J.; Myllylae, R. Comparison of the continuous wave and pulsed time-of-flight laser rangefinding techniques. *SPIE MILESTONE SERIES MS* **1995**, *115*, 280–289.
22. Wehr, A.; Lohr, U. Airborne laser scanning—an introduction and overview. *ISPRS Journal of photogrammetry and remote sensing* **1999**, *54*, 68–82.
23. Horaud, R.; Hansard, M.; Evangelidis, G.; Ménier, C. An overview of depth cameras and range scanners based on time-of-flight technologies. *Machine vision and applications* **2016**, *27*, 1005–1020.
24. Richmond, R.; Cain, S. Direct-detection LADAR systems. Society of Photo-Optical Instrumentation Engineers, 2010.
25. Amann, M.C.; Bosch, T.M.; Lescure, M.; Myllylae, R.A.; Rioux, M. Laser ranging: a critical review of unusual techniques for distance measurement. *Optical engineering* **2001**, *40*, 10–20.
26. Hansard, M.; Lee, S.; Choi, O.; Horaud, R.P. *Time-of-flight cameras: principles, methods and applications*; Springer Science & Business Media, 2012.
27. Gokturk, S.B.; Yalcin, H.; Bamji, C. A time-of-flight depth sensor-system description, issues and solutions. 2004 Conference on Computer Vision and Pattern Recognition Workshop. IEEE, 2004, pp. 35–35.
28. Möller, T.; Kraft, H.; Frey, J.; Albrecht, M.; Lange, R. Robust 3D measurement with PMD sensors. *Range Imaging Day, Zürich* **2005**, *7*.
29. Lefloch, D.; Nair, R.; Lenzen, F.; Schäfer, H.; Streeter, L.; Cree, M.J.; Koch, R.; Kolb, A. Technical foundation and calibration methods for time-of-flight cameras. In *Time-of-Flight and Depth Imaging. Sensors, Algorithms, and Applications*; Springer, 2013; pp. 3–24.
30. Lange, R.; Seitz, P. Solid-state time-of-flight range camera. *IEEE Journal of quantum electronics* **2001**, *37*, 390–397.
31. Foix, S.; Alenya, G.; Torras, C. Lock-in time-of-flight (ToF) cameras: A survey. *IEEE Sensors Journal* **2011**, *11*, 1917–1926.
32. Oggier, T.; Büttgen, B.; Lustenberger, F.; Becker, G.; Rüegg, B.; Hodac, A. SwissRanger SR3000 and first experiences based on miniaturized 3D-TOF cameras. *Proc. of the First Range Imaging Research Day at ETH Zurich* **2005**.
33. Petermann, K. *Laser Diode Modulation and Noise*; Advances in Opto-Electronics, Springer Netherlands, 1988.
34. Jha, A.; Azcona, F.J.; Royo, S. Frequency-modulated optical feedback interferometry for nanometric scale vibrometry. *IEEE Photonics Technology Letters* **2016**, *28*, 1217–1220.
35. Agishev, R.; Gross, B.; Moshary, F.; Gilerson, A.; Ahmed, S. Range-resolved pulsed and CWFM lidars: potential capabilities comparison. *Applied Physics B* **2006**, *85*, 149–162.
36. Uttam, D.; Culshaw, B. Precision time domain reflectometry in optical fiber systems using a frequency modulated continuous wave ranging technique. *Journal of Lightwave Technology* **1985**, *3*, 971–977.
37. Aulia, S.; Suksmono, A.B.; Munir, A. Stationary and moving targets detection on FMCW radar using GNU radio-based software defined radio. 2015 International Symposium on Intelligent Signal Processing and Communication Systems (ISPACS). IEEE, 2015, pp. 468–473.
38. Wojtkiewicz, A.; Misiurewicz, J.; Nalecz, M.; Jedrzejewski, K.; Kulpa, K. Two-dimensional signal processing in FMCW radars. *Proc. XX KKTOiUE* **1997**, pp. 475–480.

Peer-reviewed version available at Appl. Sci. 2019, 9, 4093; doi:10.3390/app9194093

39. Feneyrou, P.; Leviandier, L.; Minet, J.; Pillet, G.; Martin, A.; Dolfi, D.; Schlotterbeck, J.P.; Rondeau, P.; Lacondemine, X.; Rieu, A.; others. Frequency-modulated multifunction lidar for anemometry, range finding, and velocimetry–1. Theory and signal processing. *Applied optics* **2017**, *56*, 9663–9675.
40. Rasshofer, R.; Gresser, K. Automotive radar and lidar systems for next generation driver assistance functions. *Advances in Radio Science* **2005**, *3*, 205–209.
41. Williams, G.M. Optimization of eyesafe avalanche photodiode lidar for automobile safety and autonomous navigation systems. *Optical Engineering* **2017**, *56*, 031224.
42. Duong, H.V.; Lefsky, M.A.; Ramond, T.; Weimer, C. The electronically steerable flash lidar: A full waveform scanning system for topographic and ecosystem structure applications. *IEEE Transactions on Geoscience and Remote Sensing* **2012**, *50*, 4809–4820.
43. Thakur, R. Scanning LIDAR in Advanced Driver Assistance Systems and Beyond: Building a road map for next-generation LIDAR technology. *IEEE Consumer Electronics Magazine* **2016**, *5*, 48–54.
44. Council, N.R.; others. *Laser radar: progress and opportunities in active electro-optical sensing*; National Academies Press, 2014.
45. Montagu, J. Galvanometric and Resonant Scanners. In *Handbook of Optical and Laser Scanning, Second Edition*; CRC Press, 2016; pp. 418–473.
46. Zhou, Y.; Lu, Y.; Hei, M.; Liu, G.; Fan, D. Motion control of the wedge prisms in Risley-prism-based beam steering system for precise target tracking. *Applied optics* **2013**, *52*, 2849–2857.
47. Davis, S.R.; Farca, G.; Rommel, S.D.; Johnson, S.; Anderson, M.H. Liquid crystal waveguides: new devices enabled by> 1000 waves of optical phase control. Emerging Liquid Crystal Technologies V. International Society for Optics and Photonics, 2010, Vol. 7618, p. 76180E.
48. Han, W.; Haus, J.W.; McManamon, P.; Heikenfeld, J.; Smith, N.; Yang, J. Transmissive beam steering through electrowetting microprism arrays. *Optics Communications* **2010**, *283*, 1174–1181.
49. Akatay, A.; Ataman, C.; Urey, H. High-resolution beam steering using microlens arrays. *Optics letters* **2006**, *31*, 2861–2863.
50. Ayers, G.J.; Ciampa, M.A.; Vranos, N.A. Holographic Optical Beam Steering Demonstration **2010**.
51. Yoo, H.W.; Druml, N.; Brunner, D.; Schwarzl, C.; Thurner, T.; Hennecke, M.; Schitter, G. MEMS-based lidar for autonomous driving. *e & i Elektrotechnik und Informationstechnik* **2018**, *135*, 408–415.
52. Ullrich, A.; Pfennigbauer, M.; Rieger, P. How to read your LIDAR spec–a comparison of single-laser-output and multi-laser-output LIDAR instruments. *Riegl laser measurement systems GmbH* **2013**.
53. Baluja, S. Evolution of an Artificial Neural Network Based Autonomous Land Vehicle Controller. *IEEE Transactions on Systems, Man, and Cybernetics-Part B: Cybernetics* **1996**, *26*, 450–463.
54. Jo, K.; Kim, J.; Kim, D.; Jang, C.; Sunwoo, M. Development of autonomous car—Part I: Distributed system architecture and development process. *IEEE Transactions on Industrial Electronics* **2014**, *61*, 7131–7140.
55. Ackerman, E. Hail, robo-taxi![top tech 2017]. *IEEE Spectrum* **2017**, *54*, 26–29.
56. Ataman, Ç.; Lani, S.; Noell, W.; De Rooij, N. A dual-axis pointing mirror with moving-magnet actuation. *Journal of Micromechanics and Microengineering* **2012**, *23*, 025002.
57. Ye, L.; Zhang, G.; You, Z. 5 V compatible two-axis PZT driven MEMS scanning mirror with mechanical leverage structure for miniature LiDAR application. *Sensors* **2017**, *17*, 521.
58. Schenk, H.; Durr, P.; Haase, T.; Kunze, D.; Sobe, U.; Lakner, H.; Kuck, H. Large deflection micromechanical scanning mirrors for linear scans and pattern generation. *IEEE journal of selected topics in quantum electronics* **2000**, *6*, 715–722.
59. Stann, B.L.; Dammann, J.F.; Giza, M.M. Progress on MEMS-scanned ladar. Laser Radar Technology and Applications XXI. International Society for Optics and Photonics, 2016, Vol. 9832, p. 98320L.
60. Kim, G.; Eom, J.; Park, Y. Design and implementation of 3d lidar based on pixel-by-pixel scanning and ds-ocdma. Smart Photonic and Optoelectronic Integrated Circuits XIX. International Society for Optics and Photonics, 2017, Vol. 10107, p. 1010710.
61. Holmström, S.T.; Baran, U.; Urey, H. MEMS laser scanners: a review. *Journal of Microelectromechanical Systems* **2014**, *23*, 259–275.
62. Urey, H.; Wine, D.W.; Osborn, T.D. Optical performance requirements for MEMS-scanner-based microdisplays. MOEMS and Miniaturized Systems. International Society for Optics and Photonics, 2000, Vol. 4178, pp. 176–186.

Peer-reviewed version available at Appl. Sci. 2019, 9, 4093; doi:10.3390/app9194093

63. Yalcinkaya, A.D.; Urey, H.; Brown, D.; Montague, T.; Sprague, R. Two-axis electromagnetic microscanner for high resolution displays. *Journal of Microelectromechanical Systems* **2006**, *15*, 786–794.
64. Mizuno, T.; Mita, M.; Kajikawa, Y.; Takeyama, N.; Ikeda, H.; Kawahara, K. Study of two-dimensional scanning LIDAR for planetary explorer. Sensors, systems, and next-generation satellites XII. International Society for Optics and Photonics, 2008, Vol. 7106, p. 71061A.
65. Park, I.; Jeon, J.; Nam, J.; Nam, S.; Lee, J.; Park, J.; Yang, J.; Ebisuzaki, T.; Kawasaki, Y.; Takizawa, Y.; others. A new LIDAR method using MEMS micromirror array for the JEM-EUSO mission. Proc. Of the 31st ICRC Conference, 2009.
66. Moss, R.; Yuan, P.; Bai, X.; Quesada, E.; Sudharsanan, R.; Stann, B.L.; Dammann, J.F.; Giza, M.M.; Lawler, W.B. Low-cost compact MEMS scanning ladar system for robotic applications. Laser Radar Technology and Applications XVII. International Society for Optics and Photonics, 2012, Vol. 8379, p. 837903.
67. Riu, J., R.S.R.N.S.F. OPTRO2018: Proceedings of the 8th International Symposium on Optronics in Defence and Security, 2018, pp. 1–4.
68. Heck, M.J. Highly integrated optical phased arrays: photonic integrated circuits for optical beam shaping and beam steering. *Nanophotonics* **2016**, *6*, 93–107.
69. Hansen, R.C. *Phased array antennas*; Vol. 213, John Wiley & Sons, 2009.
70. Hutchison, D.N.; Sun, J.; Doylend, J.K.; Kumar, R.; Heck, J.; Kim, W.; Phare, C.T.; Feshali, A.; Rong, H. High-resolution aliasing-free optical beam steering. *Optica* **2016**, *3*, 887–890.
71. Sun, J.; Timurdogan, E.; Yaacobi, A.; Hosseini, E.S.; Watts, M.R. Large-scale nanophotonic phased array. *Nature* **2013**, *493*, 195.
72. Van Acoleyen, K.; Bogaerts, W.; Jágerská, J.; Le Thomas, N.; Houdré, R.; Baets, R. Off-chip beam steering with a one-dimensional optical phased array on silicon-on-insulator. *Optics letters* **2009**, *34*, 1477–1479.
73. Eldada, L. Solid state LIDAR for ubiquitous 3D sensing. GPU Technology Conference. Quanergy Systems, Inc., 2016.
74. Fersch, T.; Weigel, R.; Koelpin, A. Challenges in miniaturized automotive long-range lidar system design. Three-Dimensional Imaging, Visualization, and Display 2017. International Society for Optics and Photonics, 2017, Vol. 10219, p. 102190T.
75. Rabinovich, W.S.; Goetz, P.G.; Pruessner, M.W.; Mahon, R.; Ferraro, M.S.; Park, D.; Fleet, E.F.; DePrenger, M.J. Two-dimensional beam steering using a thermo-optic silicon photonic optical phased array. *Optical Engineering* **2016**, *55*, 111603.
76. Laux, T.E.; Chen, C.I. 3D flash LIDAR vision systems for imaging in degraded visual environments. Degraded Visual Environments: Enhanced, Synthetic, and External Vision Solutions 2014. International Society for Optics and Photonics, 2014, Vol. 9087, p. 908704.
77. Rohrschneider, R.; Masciarelli, J.; Miller, K.L.; Weimer, C. An overview of ball flash LiDAR and related technology development. AIAA Guidance, Navigation, and Control (GNC) Conference, 2013, p. 4642.
78. Carrara, L.; Fiergolski, A. An Optical Interference Suppression Scheme for TCSPC Flash LiDAR Imagers. *Applied Sciences* **2019**, *9*, 2206.
79. Gelbart, A.; Redman, B.C.; Light, R.S.; Schwartzlow, C.A.; Griffis, A.J. Flash lidar based on multiple-slit streak tube imaging lidar. Laser Radar Technology and Applications VII. International Society for Optics and Photonics, 2002, Vol. 4723, pp. 9–19.
80. McManamon, P.F.; Banks, P.; Beck, J.; Huntington, A.S.; Watson, E.A. A comparison flash lidar detector options. Laser Radar Technology and Applications XXI. International Society for Optics and Photonics, 2016, Vol. 9832, p. 983202.
81. Continental Showcases Innovations in Automated Driving, Electrification and Connectivity. Automotive Engineering Exposition 2018 Yokohama. Continental Automotive Corporation, 2018.
82. Christian, J.A.; Cryan, S. A survey of LIDAR technology and its use in spacecraft relative navigation. AIAA Guidance, Navigation, and Control (GNC) Conference, 2013, p. 4641.
83. Jokela, M.; Kutila, M.; Pyykönen, P. Testing and Validation of Automotive Point-Cloud Sensors in Adverse Weather Conditions. *Applied Sciences* **2019**, *9*, 2341. doi:10.3390/app9112341.
84. Yoo, H.W.; Druml, N.; Brunner, D.; Schwarzl, C.; Thurner, T.; Hennecke, M.; Schitter, G. MEMS-based lidar for autonomous driving. *Elektrotech. Inftech.* **2018**, *135*, 408–415. doi:10.1007/s00502-018-0635-2.
85. Udd, E.; Spillman Jr, W.B. *Fiber optic sensors: an introduction for engineers and scientists*; John Wiley & Sons, 2011.

Peer-reviewed version available at Appl. Sci. 2019, 9, 4093; doi:10.3390/app9194093

86. Barnes, W.; Poole, S.B.; Townsend, J.; Reekie, L.; Taylor, D.; Payne, D.N. Er3+-Yb3+ and Er3+-doped fibre lasers. *Journal of Lightwave Technology* **1989**, *7*, 1461–1465.
87. Kelson, I.; Hardy, A.A. Strongly pumped fiber lasers. *IEEE Journal of Quantum Electronics* **1998**, *34*, 1570–1577.
88. Koo, K.; Kersey, A. Bragg grating-based laser sensors systems with interferometric interrogation and wavelength division multiplexing. *Journal of Lightwave Technology* **1995**, *13*, 1243–1249.
89. Lee, B. Review of the present status of optical fiber sensors. *Optical fiber technology* **2003**, *9*, 57–79.
90. Paschotta, R. Field guide to optical fiber technology. SPIE, 2010.
91. Sennaroglu, A. *Solid-state lasers and applications*; CRC press, 2006.
92. Huber, G.; Kränkel, C.; Petermann, K. Solid-state lasers: status and future. *JOSA B* **2010**, *27*, B93–B105.
93. Zayhowski, J.J. Q-switched operation of microchip lasers. *Optics letters* **1991**, *16*, 575–577.
94. Taira, T.; Mukai, A.; Nozawa, Y.; Kobayashi, T. Single-mode oscillation of laser-diode-pumped Nd: YVO 4 microchip lasers. *Optics letters* **1991**, *16*, 1955–1957.
95. Zayhowski, J.; Dill, C. Diode-pumped microchip lasers electro-optically Q switched at high pulse repetition rates. *Optics letters* **1992**, *17*, 1201–1203.
96. Zayhowski, J.J.; Dill, C. Diode-pumped passively Q-switched picosecond microchip lasers. *Optics letters* **1994**, *19*, 1427–1429.
97. Młyńczak, J.; Kopczyński, K.; Mierczyk, Z.; Zygmunt, M.; Natkański, S.; Muzal, M.; Wojtanowski, J.; Kirwil, P.; Jakubaszek, M.; Knysak, P.; others. Practical application of pulsed "eye-safe" microchip laser to laser rangefinders. *Opto-Electronics Review* **2013**, *21*, 332–337.
98. Zayhowski, J.J. Passively Q-switched microchip lasers and applications. *The Review of Laser Engineering* **1998**, *26*, 841–846.
99. Faist, J.; Capasso, F.; Sivco, D.L.; Sirtori, C.; Hutchinson, A.L.; Cho, A.Y. Quantum cascade laser. *Science* **1994**, *264*, 553–556.
100. Chow, W.W.; Koch, S.W. *Semiconductor-laser fundamentals: physics of the gain materials*; Springer Science & Business Media, 1999.
101. Coldren, L.A.; Corzine, S.W.; Mashanovitch, M.L. *Diode lasers and photonic integrated circuits*; Vol. 218, John Wiley & Sons, 2012.
102. Sun, H. *A practical guide to handling laser diode beams*; Springer, 2015.
103. Taimre, T.; Nikolić, M.; Bertling, K.; Lim, Y.L.; Bosch, T.; Rakić, A.D. Laser feedback interferometry: a tutorial on the self-mixing effect for coherent sensing. *Adv. Opt. Photon.* **2015**, *7*, 570–631. doi:10.1364/AOP.7.000570.
104. Michalzik, R. VCSEL fundamentals. In *VCSELs*; Springer, 2013; pp. 19–75.
105. Iga, K.; Koyama, F.; Kinoshita, S. Surface emitting semiconductor lasers. *IEEE Journal of Quantum Electronics* **1988**, *24*, 1845–1855.
106. Kogelnik, H.; Shank, C. Coupled-wave theory of distributed feedback lasers. *Journal of applied physics* **1972**, *43*, 2327–2335.
107. Bachmann, F.; Loosen, P.; Poprawe, R. *High power diode lasers: technology and applications*; Vol. 128, Springer, 2007.
108. Lang, R.; Kobayashi, K. External optical feedback effects on semiconductor injection laser properties. *IEEE journal of Quantum Electronics* **1980**, *16*, 347–355.
109. Kono, S.; Koda, R.; Kawanishi, H.; Narui, H. 9-kW peak power and 150-fs duration blue-violet optical pulses generated by GaInN master oscillator power amplifier. *Opt. Express* **2017**, *25*, 14926. doi:10.1364/OE.25.014926.
110. Injeyan, H.; Goodno, G.D. *High power laser handbook*; McGraw-Hill Professional New York, 2011.
111. McManamon, P.F. Review of ladar: a historic, yet emerging, sensor technology with rich phenomenology. *Optical Engineering* **2012**, *51*, 060901.
112. Yu, C.; Shangguan, M.; Xia, H.; Zhang, J.; Dou, X.; Pan, J.W. Fully integrated free-running InGaAs/InP single-photon detector for accurate lidar applications. *Opt. Express* **2017**, *25*, 14611. doi:10.1364/OE.25.014611.
113. Capasso, F. Physics of avalanche photodiodes. In *Semiconductors and semimetals*; Elsevier, 1985; Vol. 22, pp. 1–172.

Peer-reviewed version available at Appl. Sci. 2019, 9, 4093; doi:10.3390/app9194093

114. Renker, D. Geiger-mode avalanche photodiodes, history, properties and problems. *Nuclear Instruments and Methods in Physics Research Section A: Accelerators, Spectrometers, Detectors and Associated Equipment* **2006**, *567*, 48–56.
115. Piatek, S.S. Physics and Operation of an MPPC. *Hamamatsu Corporation and New Jersey Institute of Technology* **2014**.
116. Riu, J.; Sicard, M.; Royo, S.; Comerón, A. Silicon photomultiplier detector for atmospheric lidar applications. *Opt. Lett.* **2012**, *37*, 1229–1231. doi:10.1364/OL.37.001229.
117. Nabet, B. *Photodetectors: Materials, devices and applications*; Woodhouse Publishing, 2015.
118. Yotter, R.A.; Wilson, D.M. A review of photodetectors for sensing light-emitting reporters in biological systems. *IEEE Sensors Journal* **2003**, *3*, 288–303.
119. Melchior, H.; Fisher, M.B.; Arams, F.R. Photodetectors for optical communication systems. *Proceedings of the IEEE* **1970**, *58*, 1466–1486.
120. Alexander, S.B. *Optical communication receiver design*; SPIE Optical engineering press London, 1997.
121. McManamon, P. *LiDAR technologies and systems*; SPIE Press, 2019.
122. Ng, K.K., Avalanche Photodiode (APD). In *Complete Guide to Semiconductor Devices*; IEEE, 2002. doi:10.1109/9780470547205.ch58.
123. Zappa, F.; Lotito, A.; Giudice, A.C.; Cova, S.; Ghioni, M. Monolithic active-quenching and active-reset circuit for single-photon avalanche detectors. *IEEE Journal of Solid-State Circuits* **2003**, *38*, 1298–1301. doi:10.1109/JSSC.2003.813291.
124. Cova, S.; Ghioni, M.; Lotito, A.; Rech, I.; Zappa, F. Evolution and prospects for single-photon avalanche diodes and quenching circuits. *Journal of Modern Optics* **2004**, *51*, 1267–1288. doi:10.1080/09500340408235272.
125. Charbon, E.; Fishburn, M.; Walker, R.; Henderson, R.K.; Niclass, C. SPAD-Based Sensors. In *TOF Range-Imaging Cameras*; Remondino, F.; Stoppa, D., Eds.; Springer Berlin Heidelberg: Berlin, Heidelberg, 2013; pp. 11–38. doi:10.1007/978-3-642-27523-4_2.
126. Carrara, L.; Fiergolski, A. An Optical Interference Suppression Scheme for TCSPC Flash LiDAR Imagers. *Applied Sciences* **2019**, *9*, 2206. doi:10.3390/app9112206.
127. Yamamoto, K.; Yamamura, K.; Sato, K.; Ota, T.; Suzuki, H.; Ohsuka, S. Development of Multi-Pixel Photon Counter (MPPC). 2006 IEEE Nuclear Science Symposium Conference Record, 2006, Vol. 2, pp. 1094–1097. doi:10.1109/NSSMIC.2006.356038.
128. Gomi, S.; Hano, H.; Iijima, T.; Itoh, S.; Kawagoe, K.; Kim, S.H.; Kubota, T.; Maeda, T.; Matsumura, T.; Mazuka, Y.; Miyabayashi, K.; Miyata, H.; Murakami, T.; Nakadaira, T.; Nakaya, T.; Otono, H.; Sano, E.; Shinkawa, T.; Sudo, Y.; Takeshita, T.; Taguchi, M.; Tsubokawa, T.; Uozumi, S.; Yamaoka, M.; Yamazaki, H.; Yokoyama, M.; Yoshimura, K.; Yoshioka, T. Development and study of the multi pixel photon counter. *Nuclear Instruments and Methods in Physics Research Section A: Accelerators, Spectrometers, Detectors and Associated Equipment* **2007**, *581*, 427–432. doi:10.1016/j.nima.2007.08.020.
129. Ward, M.; Vacheret, A. Impact of after-pulse, pixel crosstalk and recovery time in multi-pixel photon counter (TM) response. *Nuclear Instruments and Methods in Physics Research Section A: Accelerators, Spectrometers, Detectors and Associated Equipment* **2009**, *610*, 370–373. doi:10.1016/j.nima.2009.05.127.
130. Foord, R.; Jones, R.; Oliver, C.J.; Pike, E.R. The Use of Photomultiplier Tubes for Photon Counting. *Appl. Opt.* **1969**, *8*, 1975–1989. doi:10.1364/AO.8.001975.
131. Schwarz, B. LIDAR: Mapping the world in 3D. *Nature Photonics* **2010**, *4*, 429–430. doi:10.1038/nphoton.2010.148.
132. Gotzig, H.; Geduld, G. Automotive LIDAR. In *Handbook of Driver Assistance Systems*; Winner, H.; Hakuli, S.; Lotz, F.; Singer, C., Eds.; Springer International Publishing: Cham, 2015; pp. 1–20. doi:10.1007/978-3-319-09840-1_18-1.
133. Hecht, J. Lidar for Self-Driving Cars. *Opt. Photon. News* **2018**, *29*, 26–33.
134. Rosique, F.; Navarro, P.J.; Fernández, C.; Padilla, A. A Systematic Review of Perception System and Simulators for Autonomous Vehicles Research. *Sensors* **2019**, *19*, 648. doi:10.3390/s19030648.
135. Heinrich, S. Flash Memory in the emerging age of autonomy **2017**. p. 10.
136. Thakur, R. Scanning LIDAR in Advanced Driver Assistance Systems and Beyond: Building a road map for next-generation LIDAR technology. *IEEE Consumer Electronics Magazine* **2016**, *5*, 48–54. doi:10.1109/MCE.2016.2556878.

Peer-reviewed version available at Appl. Sci. 2019, 9, 4093; doi:10.3390/app9194093

137. Bijelic, M.; Gruber, T.; Ritter, W. A Benchmark for Lidar Sensors in Fog: Is Detection Breaking Down? 2018 IEEE Intelligent Vehicles Symposium (IV), 2018, pp. 760–767. doi:10.1109/IVS.2018.8500543.
138. Rasshofer, R.H.; Spies, M.; Spies, H. Influences of weather phenomena on automotive laser radar systems. *Adv. Radio Sci.* **2011**, *9*, 49–60. doi:10.5194/ars-9-49-2011.
139. Duthon, P.; Colomb, M.; Bernardin, F. Light Transmission in Fog: The Influence of Wavelength on the Extinction Coefficient. *Applied Sciences* **2019**, *9*, 2843. doi:10.3390/app9142843.
140. Kim, G.; Eom, J.; Choi, J.; Park, Y. Mutual Interference on Mobile Pulsed Scanning LIDAR. *IEMEK Journal of Embedded Systems and Applications* **2017**, *12*, 43–62. doi:10.14372/IEMEK.2017.12.1.43.

Sample Availability: Samples of the compounds ..... are available from the authors.